IEEE Access
Multidisciplinary | Rapid Review | Open Access Journal

Received 17 February 2023, accepted 5 March 2023, date of publication 6 March 2023, date of current version 13 March 2023.

Digital Object Identifier 10.1109/ACCESS.2023.3253772

RESEARCH ARTICLE

Modeling and Simulation of Time Domain Reflectometry Signals on a Real Network for Use in Fault Classification and Location

JAVIER GRANADO FORNÁS[1], ELÍAS HERRERO JARABA[2], (Member, IEEE), HANS BLUDSZUWEIT[1], DAVID CERVERO GARCÍA[1], AND ANDRÉS LLOMBART ESTOPIÑAN[1], (Member, IEEE)

[1]CIRCE Foundation Parque Empresarial Dinamiza, 50018 Zaragoza, Spain
[2]Department of Electronic Engineering and Communications, University of Zaragoza, 50018 Zaragoza, Spain

Corresponding author: Javier Granado Fornás (jgranado@fcirce.es)

This work was supported by the FLEXIGRID Project from the European Union's Horizon 2020 Research and Innovation Programme under Agreement No 864579.

ABSTRACT Today, the classification and location of faults in electrical networks remains a topic of great interest. Faults are a major issue, mainly due to the time spent to detect, locate, and repair the cause of the fault. To reduce time and associated costs, automatic fault classification and location is gaining great interest. State-of-the-art techniques to classify and locate faults are mainly based on line-impedance measurements or the detection of the traveling wave produced by the event caused by the fault itself. In contrast, this paper describes the methodology for creating a database and a model for a complex distribution network. Both objectives are covered under the paradigm of the time-domain pulse reflectometry (TDR) principle. By using this technique, large distances can be monitored on a line with a single device. Thus, in this way a database is shared and created from the results of simulations of a real and complex distribution network modeled in the PSCAD^{TM} software, which have been validated with measurements from an experimental test setup. Experimental validations have shown that the combination of the TDR technique with the modeling of a real network (including the real injector and the network coupling filter from the prototype) provides high-quality signals that are very similar and reliable to the real ones. In this sense, it is intended firstly that this model and its corresponding data will serve as a basis for further processing by any of the existing state-of-the-art techniques. And secondly, to become a valid alternative to the already well-known Test Feeders but adapted to work groups not used to the electrical world but to the environment of pure data processing.

INDEX TERMS Fault classification, fault location, transmission lines, time-domain pulse reflectometry, modelling networks, distribution networks.

I. INTRODUCTION

From a maintenance cost point of view, distribution system operators (DSOs) are specially concerned with reducing outage times. In a collateral way, from a commercial point of view, an indeterminate number of clients lose their power supply during these periods, and some power stations (specially distributed generation, DG) may also be affected thereby. Therefore, the location of electrical faults in distribution networks and their identification are an effective method to reduce the duration of downtime, considering that most outages are caused by faults in the distribution network [1], [2], [3]. When maintenance crews can find the problem faster due to location and identification techniques, the fault can be fixed earlier and therefore the user experience is greatly improved.

On the other hand, fault location techniques are widely used in transmission systems where each line is monitored separately. But distribution networks in real environments usually have a radial, ring, or mesh topology, with many

The associate editor coordinating the review of this manuscript and approving it for publication was Yizhang Jiang.

nodes and branches [4], [5], [6], [7], [8]. Therefore, location methods need a different approach to obtain a cost-effective system that can monitor the entire grid or an important section of it.

Additionally, it is also important to consider other specific characteristics of distribution systems, such as the presence of unbalanced loads, laterals, and different types of cables/conductors. These features affect several assumptions of location methods, reducing their performance.

It is worth mentioning a couple of significant cases: 1) IT (Isolé-Terre) networks, which are common in distribution systems. In which, location is more challenging [9] since classical impedance-based methods have substantial errors. And 2), low voltage (LV) distribution grids, which especially lack studies of fault location techniques [10]. These last networks have two important differences regarding high- and medium-voltage grids:

- Underground lines are commonly made up of unshielded wires.
- The system end points are the customer loads, so there is a variability in their impedance value.

For example, series faults [11] are caused by broken wires and increase the impedance of the affected lines. Or shunt faults [12] consisting of a contact among one phase and the ground and/or other phase/s. Distribution networks suffer mainly from shunt faults [13] and, in turn, can be classified considering the number of faulty phases and the involvement of the ground:

- Single line to ground.
- Double line.
- Double line to ground.
- Three phases.
- Three-phase to ground.

Each kind of fault causes different electrical responses and may produce less or more hazardous effects. Thus, a complete fault diagnosis method should be able to resolve not only the location of the fault point but also the kind of fault found in the distribution network [14].

In conclusion, more research is needed to find more suitable fault location techniques adapted to the special characteristics of real distribution networks, and on the other hand, more realistic scenarios and data must be created and shared. In this sense, the complexity of these scenarios must be accompanied by a comprehensive set of data where several electrical faults can be found.

So, based on the above, the contribution of the present paper is built over the next points:

1) To demonstrate the methodology to model not only a real distribution network but also the injector device (as it is the central device in our current line of research), and finally, the coupling device (to protect and isolate the injector).
2) Simulate the pre-fault and fault state of the network and obtain the network response signals.
3) Certify the sufficient quality of signals obtained to be used in post-processing to detect, locate, and classify faults.
4) And finally, creating and sharing a database of simulated signals from a real network ready to be used for future studies and by many other researchers.

II. ENVIRONMENT

Today, electrification has become one of the paradigms of our society. The technological progress that humanity is undergoing generates an unprecedented dependence on electricity.

In this context, distribution networks play a fundamental role, as a service failure can have catastrophic consequences. Examples include the dependence of telecommunications, aviation, the medical industry (which is becoming more and more technologically advanced), the arms industry and, of course, the dependence of today's society on artificial lighting.

As already mentioned, the physical principle used in this work is the TDR [15], [16]. This technique was first used in 1952 by the Japanese company Tohoku, which designed a TDR-based locator (D type - by pulse injection) for a 154 kV power grid [17].

The injected pulses propagate through the network, bounces (at each impedance change) and returns to the locator, bringing information about the state of the network.

In our case, it basically consists of performing periodic injections of pulses into the line in each of the phases of the network (R-S-T). In this way, the electrical response of the network is always updated and data-ready for further faults since if a new fault occurs, the response signal is different from the signal received when the network was operating normally.

This reflection of the pulses makes it possible to record at the injection point all the signals that ''come back'' after ''bouncing'' through the different bifurcations of the network. These signals are digitized in the injector itself so that they can be further processed.

With this method, the network responses are obtained before and just after a fault occurs. Periodic injection during normal network operation provides a ''snapshot'' of the updated network status. When the fault occurs, it is injected once more to obtain the response of the network in the fault state.

So, with the perspective of what has been said so far, we address the task of modelling a real complex distribution network in order to, subsequently, by means of simulation, be able to generate network response signals to the pulses injected into the network.

With these data, a representative database [18](which is provided for other groups to investigate with) is obtained to be further processed with different fault location algorithms [19]

In the TDR technique, high-frequency pulses are injected into the network. To do that and receive the response from the network, we use an injector and coupler devices [19].

Injectors are basically voltage sources whose output can be switched for a certain time to obtain the required pulse width.

Between the injector and the network, the coupler is placed. The coupler is basically a filter that lets high-frequency pulses through in one direction and blocks the low-frequency (50 Hz) of the mains in the other direction [21], [22].

In this work, we have modelled the injector and the real coupler used in the prototype installed in the field.

We have used PSCAD^{TM} software to model the real electrical network selected. PSCAD^{TM} is a general-purpose tool to address design and simulation tasks in the areas of power electronics, power quality analysis, protections, and electrical system planning studies.

There are other software tools that are also useful for this purpose, such as DIgSILENT^{TM}-PowerFactory^{TM}, Matlab^{TM}-Simulink^{TM}. PSCAD^{TM} has been used in the research group for years, and it was decided to use this experience in the modelling of the network of this work.

In addition to modelling a complex real network, this work has the advantage of having a prototype injector placed in it. This fact will allow us to obtain a signal database that can be used in the future to compare and validate the signals obtained by simulation.

It will also allow for validating algorithms that are developed based on the signals obtained by simulation and that can be tested with real faults occurring in the network to validate its correct operation.

III. STATE OF THE ART

Due to the nature of this article, the state of the art has been broken down into three main sections. The first section discusses the need to create more realistic environments that bring future theoretical studies closer to the real existing problems. Therefore, a change of scenario from IEEE 13 simulations to a real network is shown. However, since our data and research are deeply linked to the TDR principle, previous work related to injectors and couplers will be discussed. Finally, since our joint aim is to provide a basis for experimentation in the task of locating and classifying electrical faults, we will review the main methods used to date.

A. CHANGE OF SCENARIO: FROM BENCHMARK TEST FEEDERS TO REAL NETWORK MODELING

The IEEE 13 bus feeder [22] is a small system that is used to test distribution systems. It operates at 4.16kV, using just one source, a sin regulator, a number of short unbalanced transmission lines, and finally, shunt capacitors. Fig. 1 shows the one-line diagram of the test system.

There are multiple publications that use the IEEE 13 network to develop fault location or classification algorithms [20], [21], [22], [23]

This network may be suitable for making comparisons of different techniques or algorithms, but since it is a simulated network that does not have some correspondence with a real network, the simulations cannot be verified.

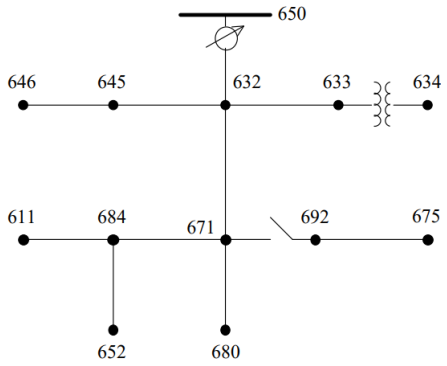

FIGURE 1. One line diagram of the IEEE 13 bus power system.

It is a very useful network for theoretical studies, where a more complex network would make it difficult to obtain clear and concise results. Frequency domain studies for harmonic minimization [24] stub line compensation [25] or studies with unbalanced loads [29]

There is a paper where the history and evolution of Test Feeders used since the 1990s is faithfully summarized [26]. Briefly, we highlight the original Test Feeder that was created in 1991, where transformers of various configurations, three-phase lines, and unbalanced loads were represented. In 1992 other models were presented at the 2000 PES Summer Meeting that were intended to become experimental platforms for unbalanced three-phase radial systems. The 13-bus Feeder [30] discussed above was published at this time along with others such as the 34-bus Feeder [30] the 37-bus Feeder [27] or the 123-bus Feeder [30]

It was not until 2010 that the 8500-Node Test Feeder was published, which aimed to scale these models to larger problems with 2500 primary buses, 4800 in total including secondary buses and loads, with a total of 8500 nodes.

In the same year, the Neutral-Earth-Voltage (NEV) Test Feeder was presented with the intention of representing very detailed models of a distribution system. It was based on a real system and contains, among other things, a line segment with 4 circuits sharing a common neutral.

For further details and study, the reader is recommended to refer to [27]

B. TDR TECHNIQUE

This work has relied heavily on the TDR technique when studying and modelling the power grid, so we see fit to review the state of the art of it by presenting works in different fields.

As stated, this technique was first used in 1952 by the Japanese company Tohoku [19]. This was the first time that an attempt was made to locate a fault in the power grid by periodic pulse injection.

In the state of the art, we find other references of TDR applied to power line fault location. In these cases, the use of this physical principle (TDR) is accompanied by another

part of the signal processing obtained through the response to these pulses. Typically, this processing consists of algorithms based on artificial intelligence [28], [29].

Also, within this same field, multiple faults have been attempted simultaneously relying on the use of this technique [30]. More recently, in the literature we can find references to the use of the TDR technique versus FDR (Frequency Domain Reflectometry), not only for the localization of faults in power lines but also in antenna cables. [31].

The popularity of this technique has led to its use in demanding fields such as automotive [32] or aviation [33], where it has been shown to increase safety in the use of these transport systems by monitoring their electrical systems.

We can even find uses for this technique in the rail sector applied to the detection of faults in railway electrical systems. For example, in [34]. The design of a portable device that uses TDR to detect short circuits or open circuits in train data cables is presented.

Even in electronic design, in [35] an analytical method is developed to check and correct the impedance based on TDR in the lines, of application in the development of printed circuit boards (PCBs).

C. LOCALIZATION AND CLASSIFICATION TECHNIQUES

Multiple techniques have been proposed to address the fault location problem. However, all methods can be grouped in three main categories: impedance measurement, travelling waves, and artificial intelligence.

1) IMPEDANCE MEASUREMENT

This methodology consists of measuring the apparent impedance at the rated frequency from a single point within the electrical network. The impedance measurement changes between a healthy and a faulty line. Moreover, the impedance variation is related to the fault distance. Therefore, if the apparent impedance is monitored during a fault occurrence, it is possible to determine the location of the fault.

The main advantage of this method is to work with steady-state values. Thus, the required acquisition device can be relatively inexpensive and simple. However, distribution networks have inherent characteristics that introduce substantial errors in this technique [9], [36], [37]:

- Nonuniformity of the lines.
- High-impedance faults, especially in IT grids.
- Radial topology leading to the multipoint location problem.
- Unbalanced loads among phases.

Furthermore, the presence of distributed generation becomes more challenging using impedance-based methods [38]. Consequently, this methodology does not seem to be the most suitable solution for location in the new paradigm of power distribution networks.

2) TRAVELLING WAVES

The well-known propagation of electromagnetic waves through transmission lines is the basis of this location method. Mainly, telegraph equations describe this phenomenon, where two important properties allow locating faults in power systems:

- Waves travel at a certain speed depending on the properties of the wire.
- Any impedance change along the line produces a partial reflection of the electromagnetic waves.

There are two main approaches to this technique:

- Measurement of the transient signal produced by the fault. This approach is widely used in transmission systems [39] where lines are monitored separately. However, in distribution networks, those transient waves experience multiple reflections due to the topology. Therefore, the signal intensity may be too low when it arrives at the locator, making it difficult to locate the origin of the fault. Many alternatives have been proposed to solve this challenge [8], [13], [37], [40], [41], [42], [43]. On the one hand, some of them require the installation of many complex and synchronised devices, thus the solution is not cost-effective. On the other hand, the single-device approaches rely on either complex mathematical transformation or grid simulations. Both solutions require offline calculation, and the latter is model-dependent.
- Injecting a high-frequency signal and measuring the reflected wavefronts. This technique is commonly named TDR. However, distribution networks have many forks where the travelling wave is reflected, hence the electrical response of the grid is complex. Several solutions [41], [42], [43] have been proposed to overcome this problem, but all require difficult boundary conditions or have not been proven to solve the problem in a real network yet.

In summary, TDR has shown good results in distribution systems, both in medium voltage (MV) and LV networks [43], but further research is needed in order to obtain a generalised and cost-effective method.

3) ARTIFICIAL INTELLIGENCE

There are several approaches within this discipline. Regarding fuzzy logic, it is still not clear what number of fuzzy functions are necessary to define the problem. Genetic algorithms introduce unacceptable uncertainties considering this application. While support vector machines and artificial neural networks seem to fit for fault location. Thus, many works can be found about applying these two methods to locate or classify faults in distribution networks, usually combined with other techniques [13], [20], [44].

However, these approaches always have the same problem: it is difficult to achieve an adequate database to train the algorithms due to the needed amount of data and the lack of measured waveforms from faulty lines. Therefore, nowadays each training is based on simulations and every proposed method strongly relies upon the grid model, requiring a retraining when any characteristic of the electrical grid changes [2], [10]. Furthermore, further investigations are

needed to increase the precision of these methods in fault location [44].

IV. THEORY

A. TELEGRAPHER'S EQUATIONS

For the study of transmission lines, the model used consists of a temporal discretization of the lines, that is, an infinitesimal analysis of the line is performed to understand the temporal and spatial evolution of both voltage and current.

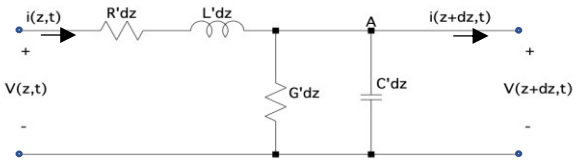

FIGURE 2. Infinitesimal portion of a transmission line.

For this purpose, the line is modelled as shown in Fig. 2, and the differential equations obtained are called the telegrapher's equations (the complete process of this model can be studied in [45].

$$\frac{\partial i(z,t)}{\partial z} + G' \cdot v(z,t) + C' \cdot \frac{\partial v(z,t)}{\partial t} = 0 \quad (1)$$

$$\frac{\partial v(z,t)}{\partial z} + R' \cdot i(z,t) + L' \cdot \frac{\partial i(z,t)}{\partial t} = 0 \quad (2)$$

The most general solution to the above equations for voltage and current is as follows:

$$v(z,t) = V^+ \cdot e^{(jwt-\gamma z)} + V^- \cdot e^{(jwt+\gamma z)} \quad (3)$$

$$i(z,t) = I^+ \cdot e^{(jwt-\gamma z)} + I^- \cdot e^{(jwt+\gamma z)} \quad (4)$$

where V^+, V^-, I^+, and I^- represent the amplitudes of the corresponding waves.

Equations (3) and (4) show that at any point on the transmission line, z, and at any instant, t, the measured voltage and current are the sum of the values of the two corresponding waves (progressive and regressive).

Thus, all the points on the transmission line experience the same variation as a function of time, the factor $j\omega t$, but with a delay due to the position, the factor γz, which will be greater the greater the distance from the origin on the z-axis. For more details, please refer to the corresponding theoretical content in [46]

B. MORPHOLOGY AND CONFIGURATION OF INJECTED SIGNALS

Taking advantage of the behavior showed in the previous section, in which the nature of the emission of a signal on a transmission line produces a return signal, we can use the latter as a "tracking" signal in search of possible disturbances in the distribution network.

In this way, electrical pulses (24 V) will be injected into the network itself, giving us updated information on the status of the network. In other words, a pulse sent to the grid in its normal state will return a series of different return signals than those that would be received when the pulse is sent when the grid is at fault.

The state of the distribution network prior to the time of the fault (with the network in its normal state) will be called the *pre-fault state*. And consequently, we will call it the *fault state* to the state of the network once the fault has occurred.

In other works, such as [44], pulses are proposed into the grid at zero crossings of the grid voltage waveform. Therefore, this imposes important restrictions on the number of pulses to be injected, mainly because the time available to inject the pulses is limited to the interval between the detection of the fault and the subsequent opening of the line breaker.

In our approach, we suppress the dependence of the injection on zero crossings and allow them to be generated at any time.

The parameters used in the implementation proposed in this article are the following:

Sampling frequency: The proposed three-phase prototype, having no limitation on the number of pulses to be injected, reconstructs the system response from the injection of four pulses, which allows one to obtain a reconstructed signal with a frequency of 100 MHz.

Injected pulse width: There is a blind zone, defined as the distance below which the proposed system is unable to locate any faults accurately. During this period of time, the system is unable to detect any disturbances or changes occurring in the power grid, which corresponds to the blind zone of the system. Therefore, to reduce the blind zone, the width of the injected pulse was reduced to 10 ns.

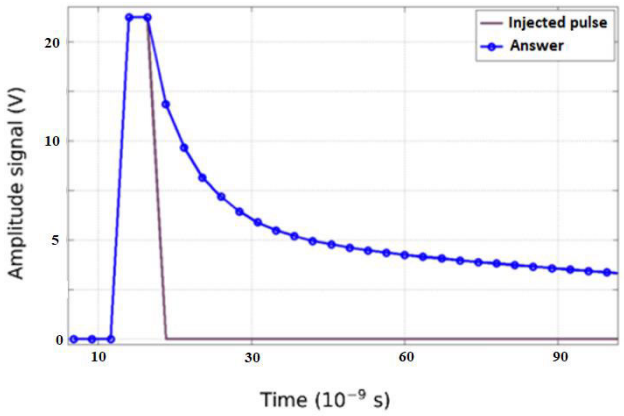

FIGURE 3. Pulse width 10 ns and response to that pulse (sampling frequency 100 MHz).

Fig. 3 shows a pulse width of 10 ns, sampled at a frequency of 100 MHz. It shows how the system response diverges at sample n=2 (taking n=0 as the instant where the pulse starts). The blind zone is calculated from the sampling frequency of the equipment (fs) and the propagation velocity of the pulse

on the line (v) according to:

$$d = n \cdot \frac{v}{2 \cdot f_s} \tag{5}$$

where n is the number of samples where the response diverges.

Therefore, consider a pulse propagation velocity of $1,65 \cdot 10^8$ m/s, and at the sampling frequency of 100 MHz, the blind zone for such a pulse is 1,65 m. However, for a pulse width of 2.5 ns, and taking the same sampling frequency and propagation speed, the first variation in the response will be seen in sample n=5, which is equivalent to 4,125 m of blind zone.

Equipment input impedance: An important addition that has been considered in our approach is the modification of the input impedance of the system. This prevents the reflected pulse from being reflected at the system connection point. In addition, to achieve a greater range when detecting or locating faults, a high impedance has been set at the input of the system.

C. NETWORK RESPONSE TO INJECTED SIGNALS

At the moment when the waveform appears, a voltage originates at the power line input, the propagation of which continues until a point of discontinuity is reached, where a change of characteristic impedance occurs, as shown in Fig. 4.

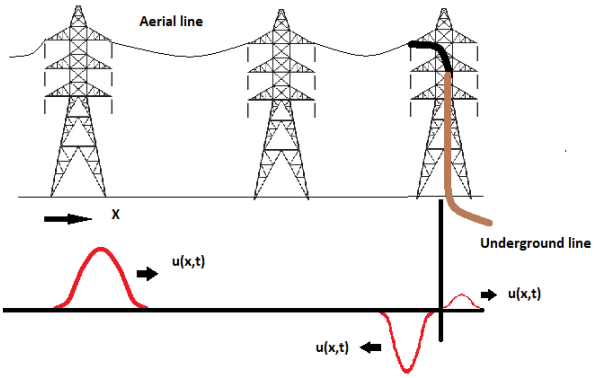

FIGURE 4. Incident, reflected, and transmitted waves at a discontinuity due to a change in impedance.

Through the characteristic impedance line Z_{0L} of the diagram in Fig. 4 an incident voltage wave u^+, and hence a current wave given by:

$$i^+(x,t) = \frac{u^+(x,t)}{Z_{0L}} \tag{6}$$

When u^+ reaches the point of discontinuity, a reflected wave u^- originates and propagates to the left, superimposing itself on the incident wave. Also, part of the incident wave is transmitted into the new medium, giving rise to a wave u^t. The continuity of the electric potential is complied with:

$$u^+(x,t) + u^-(x,t) = u^t(x,t) \tag{7}$$

Similarly, the continuity condition for the current is fulfilled at the point of discontinuity:

$$i^+(x,t) + i^-(x,t) = i^t(x,t) \tag{8}$$

Therefore:

$$\frac{u^+(x,t)}{Z_{0L}} - \frac{u^-(x,t)}{Z_{0L}} = \frac{u^t(x,t)}{Z_{0C}} \tag{9}$$

We can therefore define the reflection coefficient at the point of discontinuity as follows.

$$\zeta = \frac{u^-(x,t)}{u^+(x,t)} = \frac{Z_{0C} - Z_{0L}}{Z_{0C} + Z_{0L}} \tag{10}$$

In a zero-loss power line, these characteristic impedances do not depend on the frequency, and therefore, after transformation to the frequency domain, the reflection coefficient remains the same.

On the other hand, it follows from (10) that when the impedances of both power lines are equal, $\zeta = 0$, i.e., there is no reflected wave, and the lines are said to be matched. In the case of a short-circuit in the line, the impedance Z_{0C} can be considered as 0, so $\zeta = -1$, or in other words, $u^-(x,t) = -u^+(x,t)$, i.e. at the point where the short-circuit has occurred the entire incident wave is reflected. In the same way, it follows that, in the case of an open line $Z_{oc} = \infty$, the reflection coefficient is equal to unity, the reflected wave being twice the incident wave.

To derive equation (10), the load impedance or the characteristic impedance Z_{0C} has been considered purely resistive. However, when this impedance is reactive, the reflection coefficient in the time domain becomes a function of time and, therefore, the reflected wave $u^-(x,t)$ is defined as the convolution product between the incident wave $u^+(x,t)$ and the reflection coefficient $\zeta(x,t)$:

$$u^-(x,t) = u^+(x,t) * \zeta(x,t) \tag{11}$$

Finally, another parameter to consider would be the transmission coefficient τ, which would be defined as the relationship between transmitted and reflected waves:

$$\tau = \frac{u^t(x,t)}{u^+(x,t)} = \frac{2 \cdot Z_{0C}}{Z_{0C} + Z_{0L}} \tag{12}$$

Whose relationship with the reflection coefficient would be:

$$\tau = 1 + \zeta \tag{13}$$

V. METHODOLOGY

This section describes the methodology used to obtain response signals from an electrical network using the TDR principle. We will start by explaining our proposed system from the basic building elements (which need to be modelled accordingly), continue with the modelling of the electrical network itself, and finally, the relevant simulation process will be explained. Therefore, the following three sections will be explained in detail:

- Blocks modeling.
- Network modeling.
- Simulation process.

FIGURE 5. Methodology block diagram.

A. BLOCKS MODELING

This first section describes the basic blocks modelled (Fig. 5). It contains a generic connection to the grid, cables, loads, filters, and the pulse injector.

1) GRID CONNECTION MODEL

The system includes the CT (transformer) connection and also the MV connection, modeled with an ideal source and an R-L impedance that reflects both the Scc and the R/X ratio of the network upstream of the transformer.

Scc is the short-circuit power of the upstream MV network without CT, from which the LV model hangs and where pulses are injected.

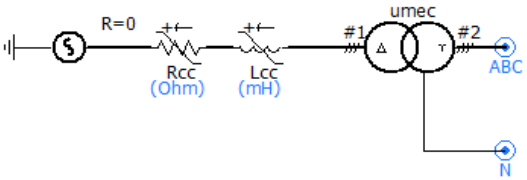

FIGURE 6. Change in impedance.

The LV network grid connection has been modelled with an adjustable RL-based equivalent load together with a transformer, as shown in Fig. 6.

The parameters of the model are:

- Short-circuit power (MVA): 20
- X/R ratio: 10
- High voltage (kV): 15
- Low voltage (kV): 0.4
- Transformer power (MVA): 0.5

The RL equivalent parameters Rcc and Lcc are calculated from the short-circuit power and the X/R ratio.

Several tests have been carried out to evaluate the impact of a variation of the R-L equivalent of the upstream MV network. The system response was tested for values of Scc = 5, 10 and 20 MVA and X/R = 10, 5 and 1. For all combinations, almost identical results were observed. Only the nominal power of the LV transformer has been found to be relevant only for the short-circuit transient, which is attenuated less with a 50 kVA transformer than with 500 kVA. Therefore, typical values have been chosen for the experiment setup.

2) LOAD MODELS

Loads are very critical in a LV network configuration, as they behave similar to faults. Load variations will cause different reflection pattern, which means that the obtained reflected signal will be very noisy. In this sense, four different load models have been implemented:

- No load (1 GΩ).
- Single-phase load.
- Symmetric 3-phase load.
- Asymmetric 3-phase load (several single-phase loads on the same bus).

The loads in the model have been derived from historical data from the active and reactive power smart meters. Average values have been converted to R and L, assuming nominal voltage. 3-phase meters were implemented as symmetric 3-phase loads. Single-phase meters are modeled as such, but on occasions, several clients are connected to the same bus. In this case, all loads are aggregated and modeled as an unbalanced 3-phase load.

3) CABLE MODELS

The grid model contains detailed models of the cables, including five different types. In LV networks, cables are not shielded, which means that HF signals travel partly outside the insulator and may have some interference with neighboring conductors. This is a fundamental difference compared to medium voltage (MV) networks, where cables are typically shielded. Geometrical cable parameters are the following:

- Number of conductors
- Conductor radius
- Insulator radius (measured from conductor center)
- Conductor distance from ground
- Conductor distances relative to each other
- Cable type: aerial or underground

All cables are considered to have 4 conductors, where the neutral wire may have a different diameter.

Apart from the geometric parameters, the frequency-dependent model has another set of parameters. The adopted values shown in table 1 have been adjusted during model

TABLE 1. Options of the frequency-dependent cable model.

Model option	Value
Travel Time Interpolation	On
Curve Fitting Starting Frequency	0.1 Hz
Curve Fitting End Frequency	1 GHz
Total Number of Frequency increments	500
Maximum Order of Fitting for Yc	20
Maximum Fitting Error for Yc	0.1 %
Max. Order per Delay Grp. for Prop. Func.	20
Maximum Fitting Error for Prop. Func.	0.1 %
DC correction	Functional Form
Passivity Checking	Disabled

testing. The fitting accuracy needed to be increased compared to the default values, in order to avoid numerical oscillations. Namely, starting frequency was reduced from 0.5 Hz to 0.1 Hz and end frequency increased from 1 MHz to 1 GHz. Frequency increments were increased from 100 to 500 and fitting errors were reduced from 0.2% to 0.1%. Finally, DC correction was modified from "Disabled" to "Functional Form".

4) PULSE INJECTOR DEVICE MODEL

The injector device mainly consists of an HF pulse generator and data acquisition with very high time resolution, which permits registration of oscillations in the nanosecond range. The pulse is created by a switch and triggered by a pulse controller. The pulse amplitude was fixed at 24 V.

Within the simulation, this controller generates one trigger before the fault event, creating the reference response, and another one after the fault event. It may be mentioned here that one trigger event consists of three triggers (one for each phase), with a time delay of 0.5 ms between them. This time delay is necessary to obtain the necessary attenuation of the pulse response, because oscillations are induced in all 3 phases.

For the pulse generator, two different options were implemented, to study the differences in response. One option was a sinusoidal signal of one period, and the other one was a rectangular pulse of half-period duration. With a pulse frequency of 1 MHz, this means that the pulse has a duration of 500 ns.

Simulation tests revealed that an ideal rectangular pulse was not suitable. Due to the detailed time-domain model, infinite ramps create singularities, and the model did not converge. Therefore, a more realistic pulse was implemented where the switch is modelled as a controllable resistance with a defined pulse.

"on" resistance (R_{on} fixed at 10 mΩ) and "off" resistance R_{off}. A ramp rate defines how fast the transition between Ron and R_{off} will occur. In the model (Fig. 7), this realistic switch model received two parameters:

- R_{off}: 1 MΩ ("off" resistance of the switch)
- ramp rate (200 ns from low to high)

These two parameters have been adjusted together with the network filter (see next section), in order to minimize oscillations induced by the switch.

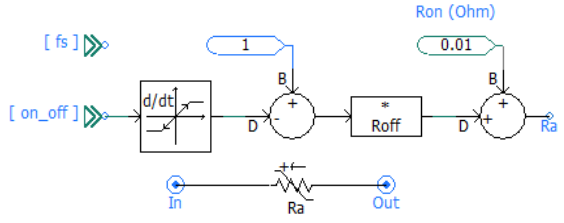

FIGURE 7. Realistic switch model with controlled switch ramps.

5) COUPLER DEVICE MODEL

The injector device is connected to the network through a filter called "Coupler" which aims to remove the grid frequency (50 or 60 Hz) and harmonics. A simple high-pass L-C filter has been used for this purpose in the model (Fig. 8). The desired design frequency of 100 kHz can be obtained from many possible combinations of L and C. Tests have shown that many combinations, especially with a large capacitance, cause oscillations when the 1-MHz pulse signals are injected.

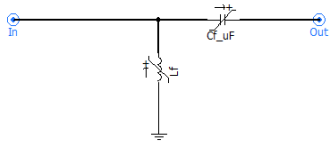

FIGURE 8. Realistic L-C network filter.

Oscillations could be reduced to an acceptable level by designing the high-pass filter with L-C values of 25.3 μH and 100 nF respectively. Note that these values are only valid together with the ramp parameters of the switch. Therefore, in a real device, filter design will be very critical. Figure 9 shows the Bode plot response diagram of the filter.

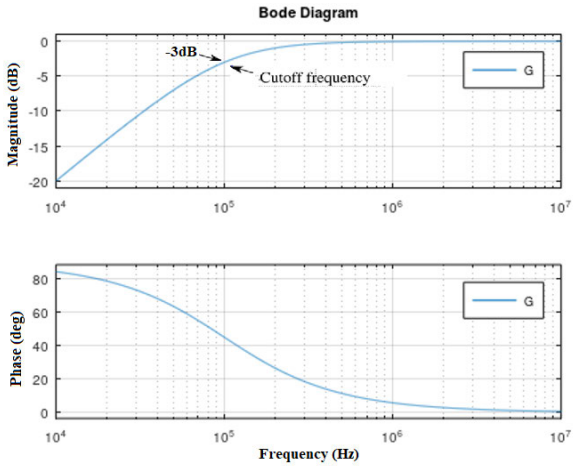

FIGURE 9. Filter-Bode plot response diagram.

B. NETWORK MODELING

This section describes the network modelled. It contains the relations between the basic blocks of the previous section. A diagram of the real network modeled is shown in Fig. 10.

Subsequently, each of the elements that have been modeled in this schematic are described one by one, allowing a simulation of the real network. This elements including the locator, which contains the pulse injector, the network coupling filter, the modeling of the network cables (with the real parameterization of each cable so that they behave like the real one), the modeling of the faults, the modeling of the loads, etc. All these elements make it possible to subsequently

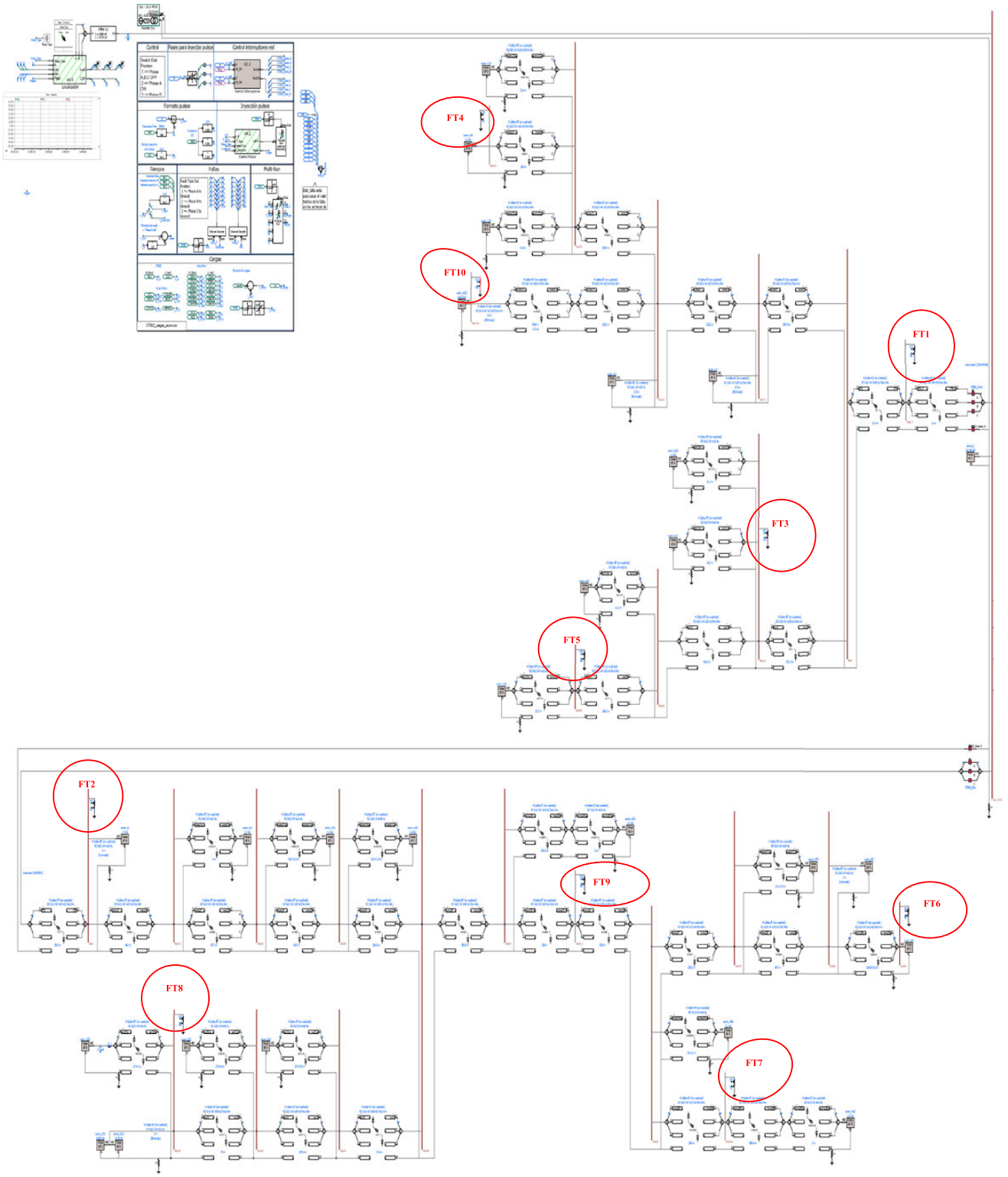

FIGURE 10. Diagram of the real network modeled.

launch simulations that allow obtaining signals very similar to these of the real network.

As we were simulating a real network, very short line segments were present in the model (below 1 m). These segments had to be eliminated or increased to a minimum length of 3 m, which was found to be a good compromise of model accuracy and simulation time. Another issue was the numerical stability of the model, depending on the grounding

resistance of the neutral. A minimum resistance of 5 Ohm was found to lead to a stable simulation.

The diagram shows the following elements:

1) FAULT LOCATOR

This is the element that injects the pulses and subsequently digitizes the network response signals (Fig. 11). These signals return after bouncing in all impedance changes (loads, bifurcations, cable type changes, faults, etc…).

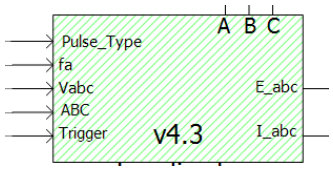

FIGURE 11. Fault locator.

Inside this block (Fig. 12), you can see the pulse injector circuit for phase A, with continuous source Va (pulse), and phase selection (switch A). The "pulse A" signal triggers the injection and comes from the "trigger" input.

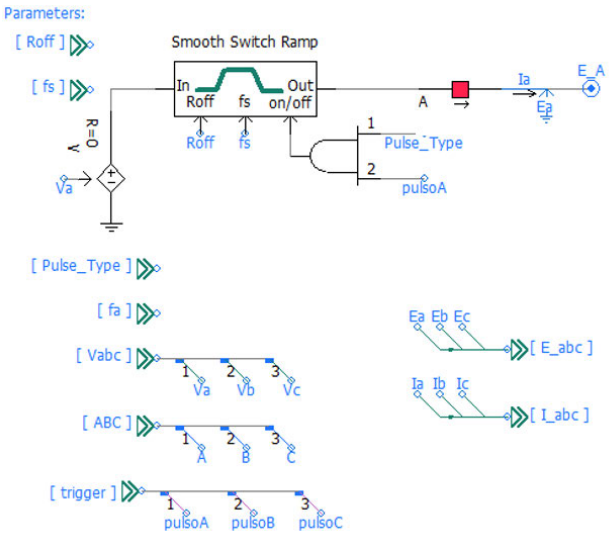

FIGURE 12. Inner fault locator.

The Fig. 7 shows the inner of the smooth-switch Ramp block.

PSCAD models the electronics (transistors, IGBTs, etc.) as ideal switches (no ramping). It has been observed that this introduces extreme transients in the model, especially when a pulse is injected. The mains LC filter has been identified as the cause, which has some sensitivity to high dU/dt ramps. Adjusting the L and C values of this filter, the effect can be minimized, but not eliminated.

To solve this problem, a new module called "Smooth Switch" has been created as an element to connect and disconnect the source to inject the pulse. This element is intended to create a more realistic pulse with controlled edges to avoid extreme ramps.

2) L-C NETWORK FILTER

The element shown in Fig. 13 represents a decoupler device (see previous section) that is placed between the injector and the mains as an insulator against the mains voltage. It is a filter for the mains frequency (50 or 60 Hz) but allows high-frequency pulses to pass in both directions.

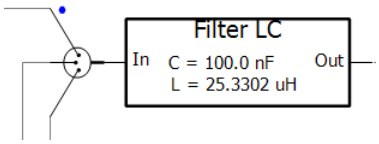

FIGURE 13. L-C network filter.

3) DETAIL OF THE NETWORK SECTION (FEEDERS)

The bifurcation, the distance of the section, the type of cable used, and the type of load at the end of the feeder are shown in Fig. 14, including the cable model and the load model. In our actual modelled grid, we have 38 feeders as it can be seen in Figure 10.

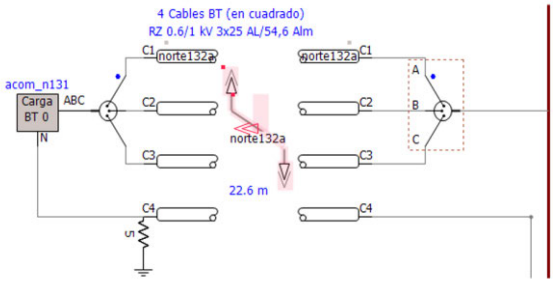

FIGURE 14. Detail of the network section.

4) DEFINITION OF FAULTS

The faults can be placed at any point on the network. Their impedance value and type can also be defined. Fig. 15 shows

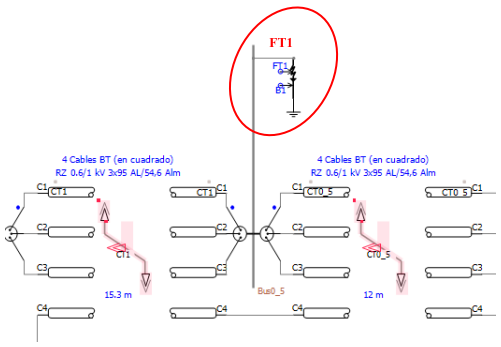

FIGURE 15. Fault FT1 in the middle of a cable run.

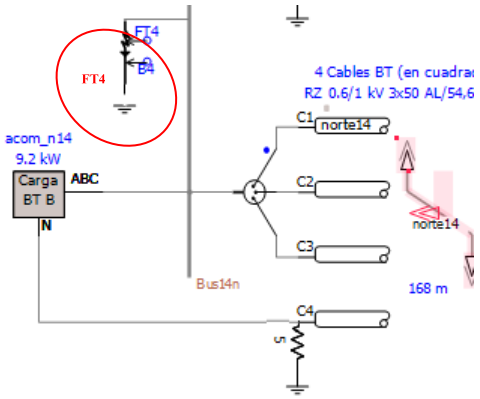

FIGURE 16. FT4 failure at the end of the run and before the load.

a fault (FT1), placed in the middle of a cable run, and Fig. 16 shows a fault (FT4), placed at the end of the run before the load.

C. SIMULATION PROCESS

1) SIMULATION PARAMETERS

This section explains all the parameters that can be set when performing a multi-run simulation.

Types of faults: Up to 10 different fault types can be defined in the simulation (Table 2):

TABLE 2. Combinations of the fault types.

Fault Type Dial Position
1 => Phase A to Ground
2 => Phase B to Ground
3 => Phase C to Ground
4 => Phase A,B to Ground
5 => Phase A,C to Ground
6 => Phase B,C to Ground
7 => Phase A,B,C to GRD
8 => Phase A,B
9 => Phase A,C
10=> Phase B,C

Position of the fault: The faults can be placed at any point on the network. In our case, we have placed 10 faults at different distances from the injector (Table 3):

Impedance of the fault: Different types of impedance can be associated with each of the defined faults. In our case, we have defined four impedance values (Table 4), ranging from a very low impedance fault or short circuit (0.01Ω) to a high impedance fault (1000 Ω):

Load values: Each of the network loads can be modeled as a resistance plus an inductance. In our case, since it is a real network, the actual data of the existing loads have been used (Fig. 17).

Injected pulse values: The injected pulse can be parameterized by varying its width, amplitude, and time delay between phases (Fig. 18).

Injection time values: The pulses can be parameterized to be injected at the most convenient time in each case. The fault event time can also be fixed(Fig. 19).

TABLE 3. Location of the faults in the simulation network.

Number of Fault	Name of bus	Distance from TDR (m)
1 (FT1, B1)	Bus0_5	12
2 (FT2, B2)	Bus2	40
3 (FT3, B3)	Bus11s	283
4 (FT4, B4)	Bus14n	933
5 (FT5, B5)	Bus13s	757
6 (FT6, B6)	Bus29n	1833
7 (FT7, B7)	Bus261n	1274
8 (FT8, B8)	Bus23s	594
9 (FT9, B9)	Bus25_5n	968
10 (FT10, B10)	Bus122n	520

TABLE 4. Impedance values.

1	0.01 Ω
2	80 Ω
3	150 Ω
4	1000 Ω

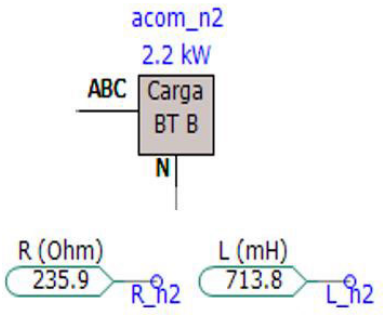

FIGURE 17. R and L are the load n2 values.

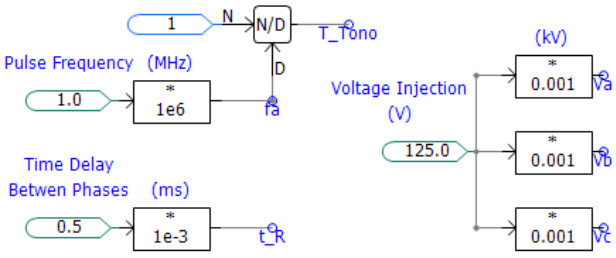

FIGURE 18. Voltage (V) and pulse rate (MHz).

Miscellaneous simulation time considerations: The simulation process starts with a waiting time of about 0.04s to reach the steady state. This process is necessary because the simulator starts the process by abruptly imposing the defined voltage on the line.

Once the steady state has been reached, a pulse is injected into each phase (R-S-T) at defined width and amplitude.

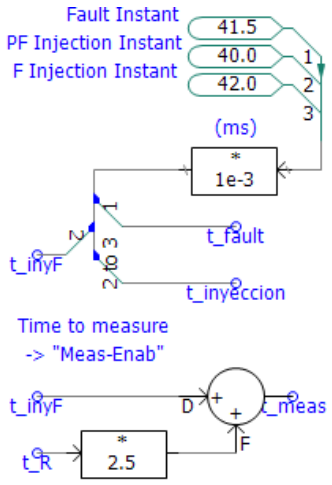

FIGURE 19. Injection time parameters.

Pulses injected in one phase can be induced in adjacent phases. To avoid this problem, it is necessary to wait until the pulse in one phase is extinguished before injecting it in the next phase. This time depends on several factors such as pulse voltage, pulse width, and the line response itself. This value is adjusted by trial and error with only one simulation case before launching all final simulations.

The simulation of each case needs about 160 s of execution time (running in Intel Core i7 7th gen).

This time is for the specific case of the real network simulated in this work.

The more complex the network, the more runtime each simulation needs.

The total number of simulated faults and the total time required for the simulation can be calculated as follows:

- Having 14 fault locations in the network. These locations have been chosen to have a wide range of distances to the injector and at various bifurcations.
- with 10 different types of fault.
- and 6 possible types of injection that arise from the combination of the number of phases in which we inject: Inject in all three phases, two by two or one by one.
- and finally, a range of fault impedances from 0.01Ω to 1000Ω. Making 5Ω steps, we have 200 values for each fault.

According to (14), as shown at the bottom of the page, with all these data, if we wanted to simulate all combinations, the complete simulation to obtain 168,000 examples would cost almost a year. It is a major problem with respect to simulating a real network. This is especially true for those classification or localization techniques based on neural networks because these types of technique require a large number of examples for training.

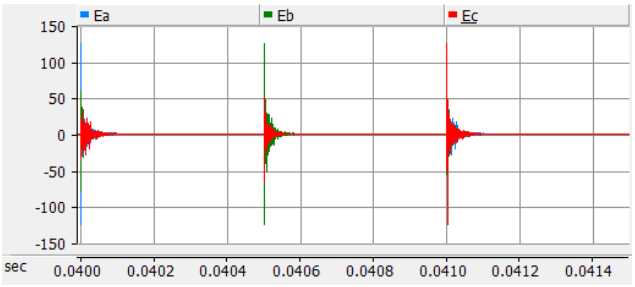

FIGURE 20. Snapshot of the pre-fault reference pulse response.

D. RESULTS OF SIMULATION RUNS

With the model set up and all design values adjusted, a multirun simulation plan was developed to create a number of different scenarios that can be feasibly simulated in a reasonable amount of time.

Bearing in mind that it must be possible to repeat the simulation in order to modify any of the parameters, we decided to select the following.

- 10 different fault locations within the network, covering cases of faults at different distances.
- 4 fault resistances: 0.01, 80, 150 and 1000 Ω
- 5 types of failures:
  - Phase-to-ground (R) -Type 1
  - Phase-to-ground (S) - Type 2
  - 2 phases-to-ground (S-T) -Type 3
  - 3-phase-to-ground (R-S-T) -Type 4
  - 2 phases-to-ground (R-S) -Type 5

All combinations were simulated, obtaining a total of 200 results.

Considering that each simulation costs about 160s, the 200 simulations take about 9 hours. This gives us a reasonable margin to run different simulations until we get the one that best suits our needs.

The simulation time step was 10 ns, and results were saved at a sample rate of 50 ns. Before starting the multiple run, the pre-fault references are obtained from a separate simulation.

A snapshot (data acquisition) with a duration of 1.51 ms is saved after 40 ms, when stationary conditions are reached. A reference response is obtained for each type of pulse.

The figures 20 and 21 show the result of one of the 200 simulations carried out (Node 1, Fault R to Ground and R_fault = 0.01 Ω) on the real simulated network. Figure 20 shows how the response to a network pulse is simulated first

$$\frac{14\,(nodes)\times 10\,(fault\ types)\times 200\,(impedance\ values)\times 6\,(Injection\ types)\times 160s}{3,600s\times 24h}=\frac{168,000\,(samples)\times 160s}{3,600s\times 24h}=311\ days \tag{14}$$

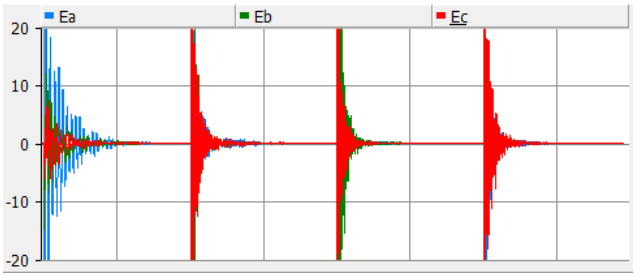

FIGURE 21. Example of pulse responses after a fault event (x: 250 μs/div, y: 10 V/div). Snapshot of the pre-fault reference pulse response.

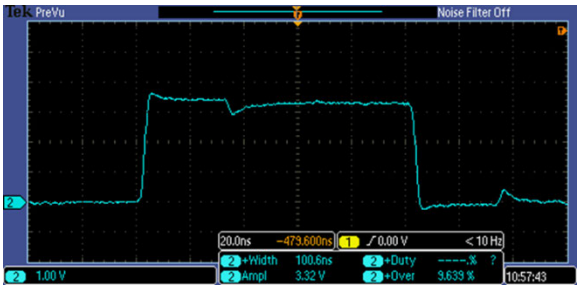

FIGURE 22. Injection pulse width = 100 ns.

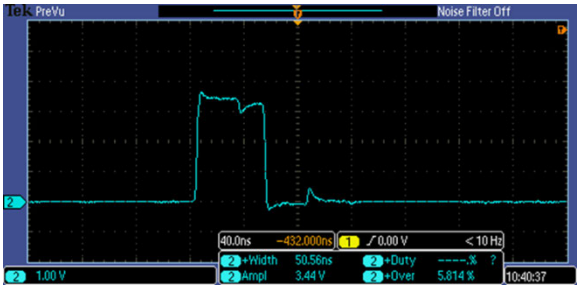

FIGURE 23. Injection pulse width = 30 ns.

before the fault occurs. It can be seen how it is injected each time in one of the phases (R-S-T labelled as Ea-Eb-Ec in the simulation software) and waits for the response to be extinguished, since the signals are normally induced in the other phases. In this way, the pulse is injected, its response is recorded, it waits for it to die out and is injected in the next phase, until completing the three injections (one of each phase). Each of the responses is concatenated to have a single network response signal before the fault (which is what is seen in the figure). Similarly, in Figure 21, the same process is seen, but before injecting, the occurrence of a fault is simulated. This signal is the first one seen in the figure and is the result of the spike that appear on the line at the moment the fault occurs. After waiting for the effects of the fault to die out, the three pulses (one in each phase) are injected in the same way as before the fault.

Finally, from the 200 simulation runs snapshots are created with a slightly longer time interval (2.01 ms), since the fault event itself is also included..

Each snapshot was saved in csv text format, and all snapshots together formed the basis for creating the database of fault signals.

VI. RESULTS

As we have no real and significant signals of faults, since we have to wait for them to occur naturally, we are going to carry out some experiments to check the validity of the work done.

The results of these experiments will be structured in four sections.

First, we are going to study the real signals available to us. On the one hand, we will compare a signal on a real single line measured with the oscilloscope against a simulated signal (section A and B). We will also compare a signal injected into the real network in normal operating state (no fault) against a simulated signal under the same conditions (section C).

Subsequently we will perform studies on simulated signals. First, we will see the behavior of the signal in a simple line without bifurcations and we will do another test in the presence of simple bifurcations in a line and putting a fault in the line to see its response (sections D and E).

We also want to see how the response of the network varies with different parameters of the simulation (fault impedance and pulse width) (sections F and G).

Finally, we will make a temporal and frequential study on the set of 200 simulated signals over the entire simulated network to draw conclusions about the information that can be extracted from them (section H).

A. STUDY OF REAL SIGNALS INJECTED IN A SINGLE SECTION WITHOUT BIFURCATIONS

The purpose of this experiment is to test the performance and validity of the injector model in a simple environment such as a single line without bifurcations.

This validation is done with a visual study of the dynamics of the response of this simple infrastructure. This similarity can be seen between the group of figures 22 to 24, and figure 26. To do this, we have performed several tests injecting pulses into a simple line formed by a coaxial cable connecting the signal injector with the oscilloscope.

The injector has an output impedance of 50 Ω, while the oscilloscope has an input impedance of 1 MΩ.

According to theory, since there is an impedance mismatch between the injector and the impedance of the oscilloscope (which here plays the role of an open line end with impedance), part of the injected signal must bounce back and return to the injector.

Fig. 22, 23 and 24 show how, after injection of a positive signal edge, a signal appears after a time according with the distance of the wire length connecting the injector and the oscilloscope. This is due to the bounce of the signal against the oscilloscope input impedance change. This property is very useful for the task of fault localization.

This signal is of opposite sign to the injected signal and of much lower amplitude. The time in which it appears is in

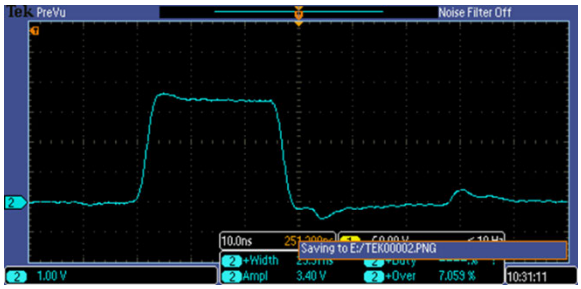

FIGURE 24. Injection pulse width = 50 ns.

FIGURE 25. Simulation of a simple line 2.5 m long.

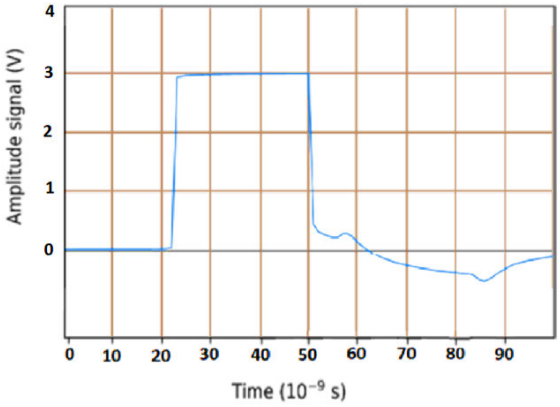

FIGURE 26. Line response to a 30 ns pulse.

accordance with the distance of the cable between the injector and the oscilloscope.

It is also observed that there is a signal bounce for each edge. One bounce is a consequence of the injection of the positive edge of the signal and another as a consequence of the negative edge.

In Fig. 24 even shows that, if the pulse width is sufficiently small, the two bounces appear once the pulse has finished, and each bounce appears approximately 35 ns from the signal that originated it. This reflection time changes according to the distance of the cable used.

In our case for a cable length of 2.5 m, considering that the propagation speed of electric current in such a cable is 0.7 c (where c is the speed of light) and that the pulse has to travel three times the length of the cable (pulse going to the oscilloscope, bouncing to the injector and bouncing to the oscilloscope again) to be "seen" by the oscilloscope. According to (15), the length L of the cable would be 2.5 m.

$$L = \frac{t_p \cdot 0.7c_0}{N} = \frac{35 \cdot 10^{-9}[s] \cdot 0.7 \cdot 3 \cdot 10^8[\frac{m}{s}]}{3} = 2.45m \tag{15}$$

B. STUDY OF SIMULATED SIGNALS IN A SINGLE SECTION WITHOUT BIFURCATIONS

In this experiment, we try to reproduce the pulse bounce phenomenon to check whether our simulation is correct.

Fig. 26 shows how in the simulation we have injected a pulse of 30 ns width and 3v amplitude. The two bounces appear once the pulse has finished approximately 35 ns later.

It can be seen that the signal is similar to the one in Fig. 24. The differences are due to the different behavior of the cable and the simulated generator with respect to the real one.

C. COMPARATIVE STUDY BETWEEN SIMULATED AND MEASURED SIGNALS

This section shows a comparison between the response to an injected pulse (in its normal state without fault) in the modeled network and the real network (Fig. 27 and Fig. 28) where the prototype injector has been installed.

The injector is placed at the same point in the network. It can be seen that the signals have a similar appearance in the time domain.

In the frequency domain, it can be observed that the real signal contains a spectrum richer in frequencies, in any case the simulation shows a good approximation to the real network.

However, the discrepancies between the two signals are expected since the modeled network is in a given state with the impedances (loads) in that state during the pulse injection.

In the real network response, the network is, in general, in a different state from that of the simulation. For this reason, in this TDR technique, pulses are constantly injected into the pre-fault state. Thus, the "picture" of the current state of the network is obtained. When the fault occurs, a pulse is injected again, and that response is processed together with the pre-fault one. In both cases, the state of the network is the same and, in variations, will be the information of the type and the distance to the fault.

This information can be extracted by the appropriate algorithms. Fig. 29 shows the actual field-assembled.

prototype with which the real signals have been injected. Fig. 30 and Fig. 31 shows the real installation on field.

The prototype will be in operation collecting signals for one year. During this period, it will record both the signals of the network in its fault-free operating state, as well as the faults that occur in the network. While these signals are being recorded, a fault location algorithm will be developed based on the database of 200 signals obtained in this work and the 10,000 synthesized signals obtained from these 200 that have been published [47] and whose database has been shared [18]. These results will be published and will also contain the error between the simulated, synthesized, and real signals obtained in the real network.

This prototype is a work of the CIRCE research group and will be presented at a congress that is in the process of being developed.

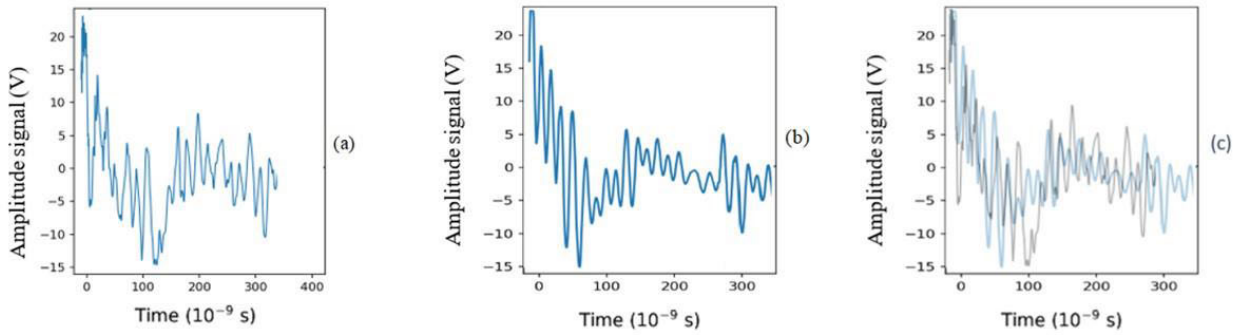

FIGURE 27. Time-domain network response to an injected pulse (a) real, (b) modelled and (c) superimposed signals.

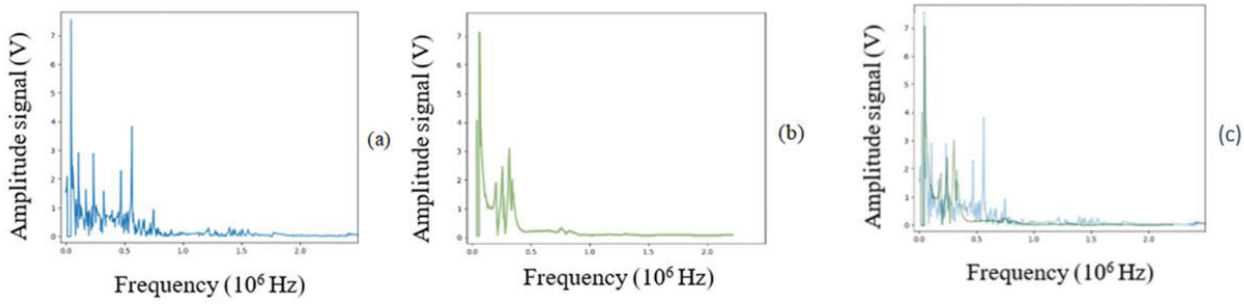

FIGURE 28. FFT network response to a pulse injected. (a) real, (b) modelled and (c) superimposed signals.

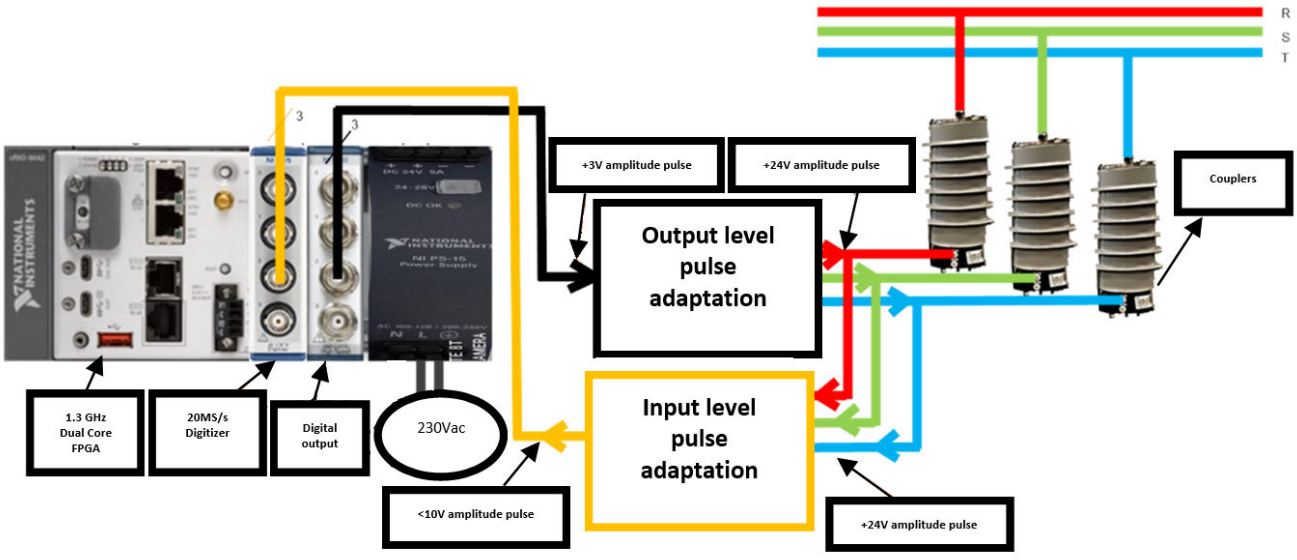

FIGURE 29. Schematic of the real prototype installed.

D. STUDY OF SIMULATED SIGNALS IN A 300 m LONG SIMPLE SECTION WITHOUT BIFURCATIONS

In this experiment, we try to reproduce the pulse bounce phenomenon to check whether our simulation is correct.

Fig. 32 shows how in the simulation we have injected a pulse of 250 ns ($5{\times}50 \cdot 10^{-9}[s]$) width and 24v amplitude, and a propagation speed in this case of 0.63 c. After about 3150 ns ($63{\times}50 \cdot 10^{-9}[s]$), the pulse bounce appears at the end of the line.

According to (16), the distance to the end of the line L is:

$$L = \frac{63 \times 50 \cdot 10^{-9}[s] \cdot 0.63 \cdot 3 \cdot 10^{8}[\frac{m}{s}]}{2} = 297m \quad (16)$$

which is consistent with the length of the simulated line.

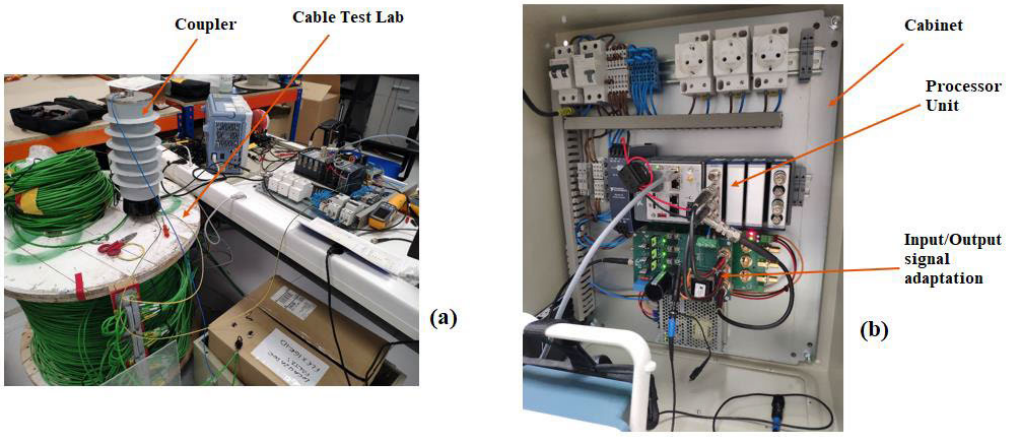

FIGURE 30. Test in lab of the prototype over single cable line (a). Fig. 1. Prototype elements in the final cabinet ready to install in field (b).

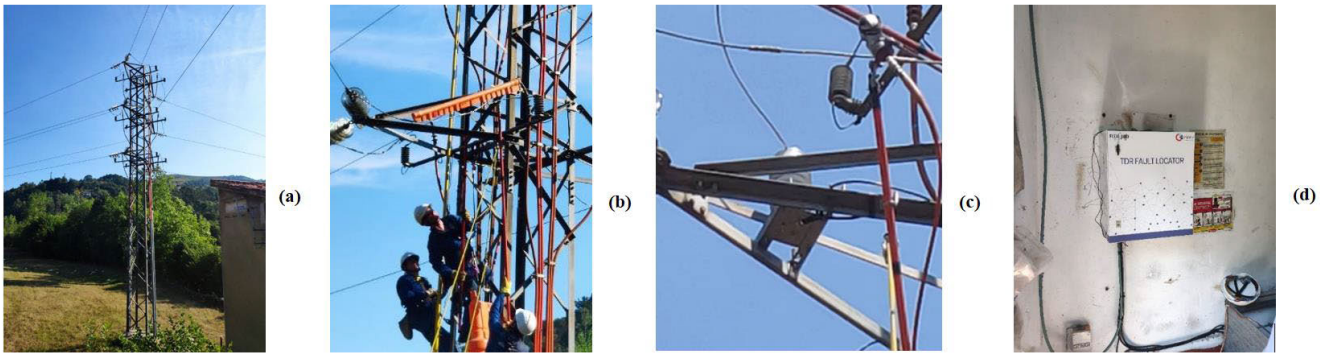

FIGURE 31. Pictures of the installation. Post where the pulses will be injected (a). Preliminary works for live installation (b). Installation of the couplers (c). Prototype cabinet installed inside the transformer station near to the post(d).

FIGURE 32. Simulation of a simple line 300m long.

E. STUDY OF SIMULATED SIGNALS IN A SECTION WITH BIFURCATIONS

This section shows (Fig. 35) the response of a bifurcated network (Fig. 34).

A fault has occurred on this line at 1100 m. The upper part of the figure shows the response of the network without fault, in which it is possible to distinguish perfectly the rebound generated at the bifurcation and the one coming from the end of the line. The lower half of the figure shows the presence of a negative sign rebound, which starts around 1100 m, the distance at which the fault occurred.

In Figure 35 (a), we can see the impedance changes that the injected pulse undergoes. first there is the bifurcation, in which part of the injected signal continues and part is reflected. Then, there is the end of line in which the signal bounces depending on the impedance of the end of line. In Figure 35 (b), we can see the same response as the previous one (with the bifurcation and the end of line), but this time, in addition, we can see how in the middle, there is another impedance change due to the fault occurred at that point (with a certain value of Z), which makes part of the signal is reflected and part continues to the end of line. The response of the section after the fault is not the same as in the previous one (a), because the signal traveling from the fault to the end of line is not the same as in the previous case, where there was no fault and the signal after the bifurcation did not suffer any impedance change.

F. IMPEDANCE INFLUENCE IN THE RESPONSE TO THE INJECTED

Fig. 31 shows the response of a single line without bifurcations to the cases of open-circuit and short-circuit line end.

In the open circuit case, the pulse reaches the end of the line and the bounce generated is of the same sign as the incident signal. In contrast, in the case where the end of the line is short-circuited, the reflected signal has the opposite

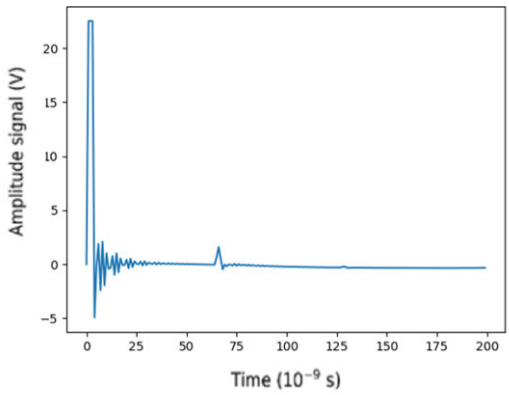

FIGURE 33. Line response to a pulse.

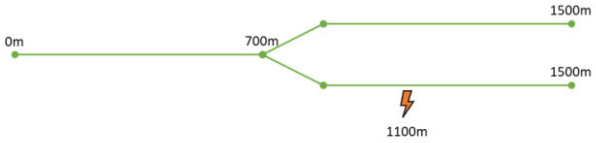

FIGURE 34. Simulation of bifurcation line.

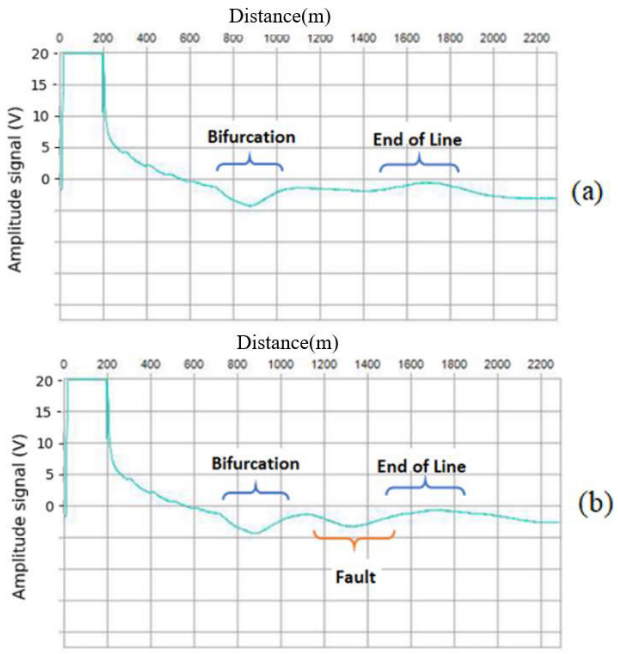

FIGURE 35. Pulse response of bifurcation line (a) without fault and (b) with fault.

sign to the incident signal, and the injector registers a negative pulse. These results confirm the theory of refraction of signals generated in line impedance changes.

G. INFLUENCE OF PULSE WITH

As already explained, the proposed localization technique is based on the reflectometry phenomenon and uses the

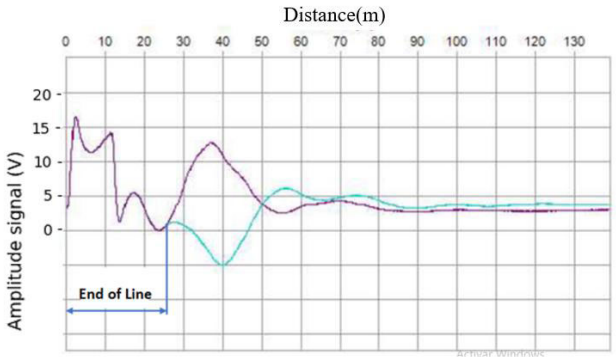

FIGURE 36. Influence of end-line impedance value.

comparison of the network response to a given signal during the pre-fault (PF) and fault (F) states. To evaluate this difference, the "error signal" (E) is defined as the arithmetic difference, sample to sample, between the two signals, both being synchronized at the instant of injection of their respective signals.

The graphs in Fig. 37 show the error signal of the three phases (R-S-T) superimposed. the response after the fault occurs. It can be seen how at the beginning, the error signal is practically null (or of a very small value), since up to the point where the fault has occurred, the signals bounced before the fault and after the fault are practically identical and begin to differ from the point where the fault has occurred.

For the determination of the pulse width, simulations of low-impedance faults have been performed at different locations in the network.

Fig. 37 shows the comparison of four simulations employing different pulse widths while keeping all other conditions constant. As can be seen in the image, the amplitude of the received signal increases with pulse width, so that a longer time on high of the injected pulse will amplify the received signal, facilitating the measurement of more distant faults.

This amplification occurs up to a certain point, since if the pulse width is increased too much, its characteristic frequency will approach the cutoff frequency of the network filter and will be attenuated by it. In this case, it has been detected that the maximum received amplitude occurs for a pulse width of 2 μs (Fig. 37 (c)).

H. TEMPORAL AND FRECUENCIAL STUDY OF THE SIMULATED SIGNALS

Finally, we analyse the simulated signals to determine whether fault information is present in the signals and can be amenable to extraction. Next, we will explain the content of each figure and the process we have followed with the injected signals.

Each figure consists of three parts. The subfigure (a) is the complete time response of the network to the injection of a pulse. At the top is the R phase, in the middle is the S phase and at the bottom is the T phase.

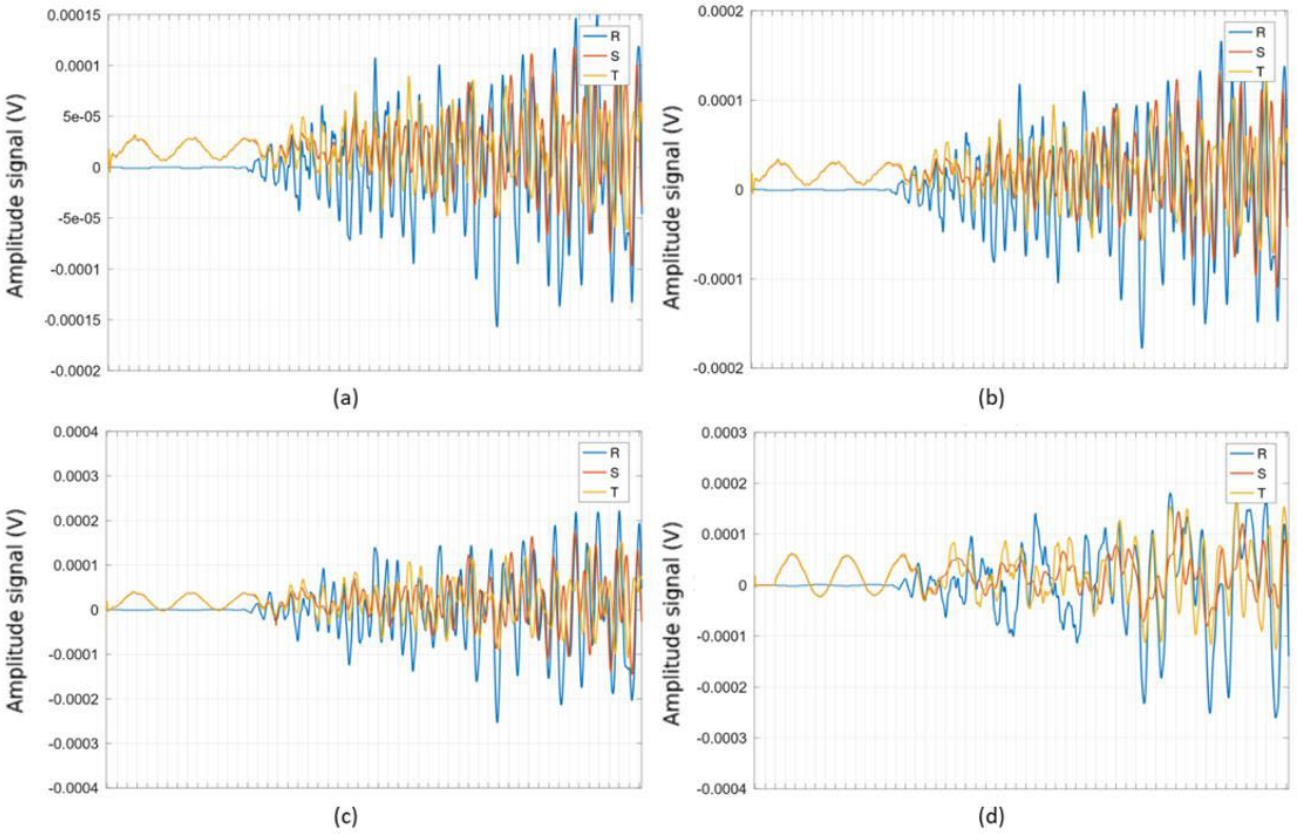

FIGURE 37. Error signal in phases R, S and T, for a low impedance fault located at a distance of 594 m in the network model for a pulse width of: (a) 0.5 μs, (b) 1 μs, (c) 2 μs, (d) 10 μs.

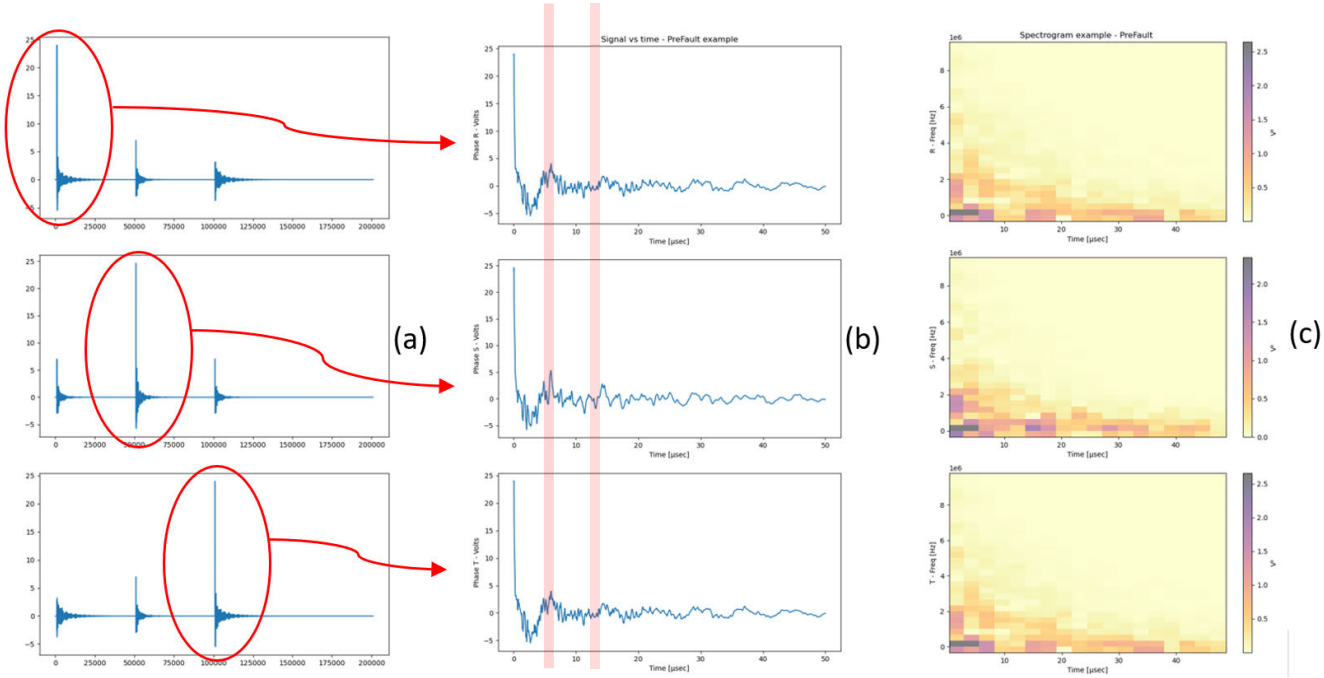

FIGURE 38. Pre-Fault signal (Top-Phase R / Middle-Phase S / Bottom-Phase T). (a) Complete Injection, (b) Phase Injection, (c) Spectrogram.

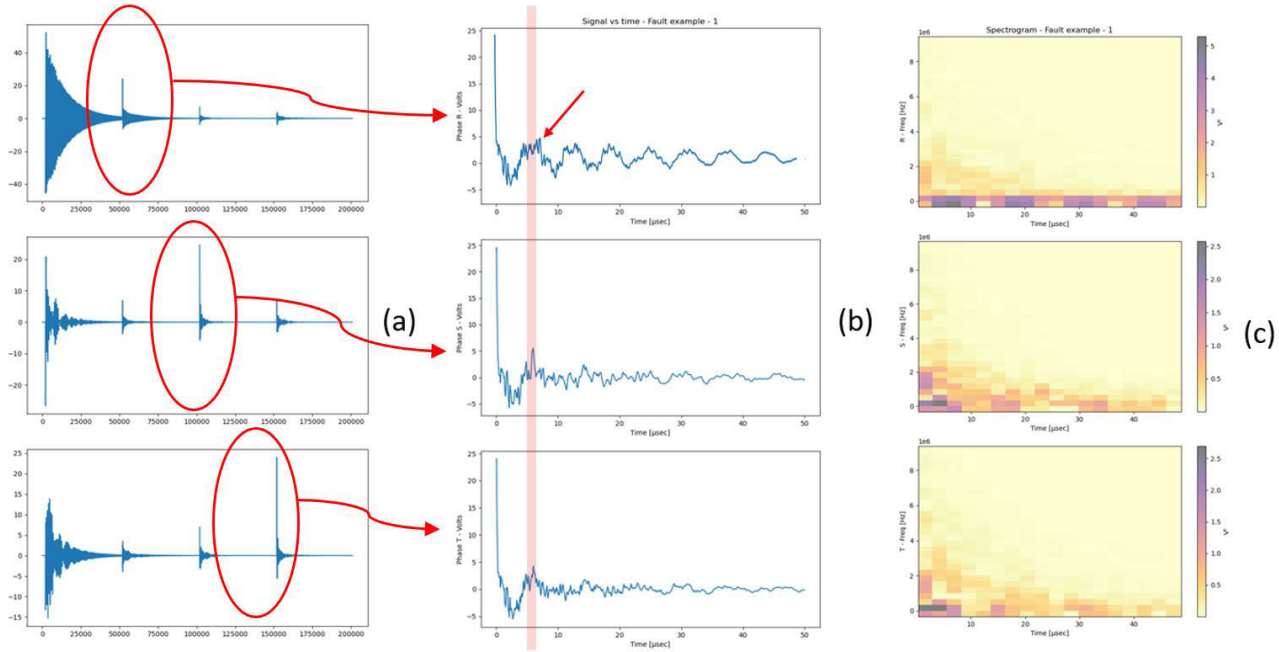

FIGURE 39. Fault signal Type 1 (Top-Phase R / Middle-Phase S / Bottom-Phase T). (a) Complete Injection, (b) Phase Injection, (c) Spectrogram.

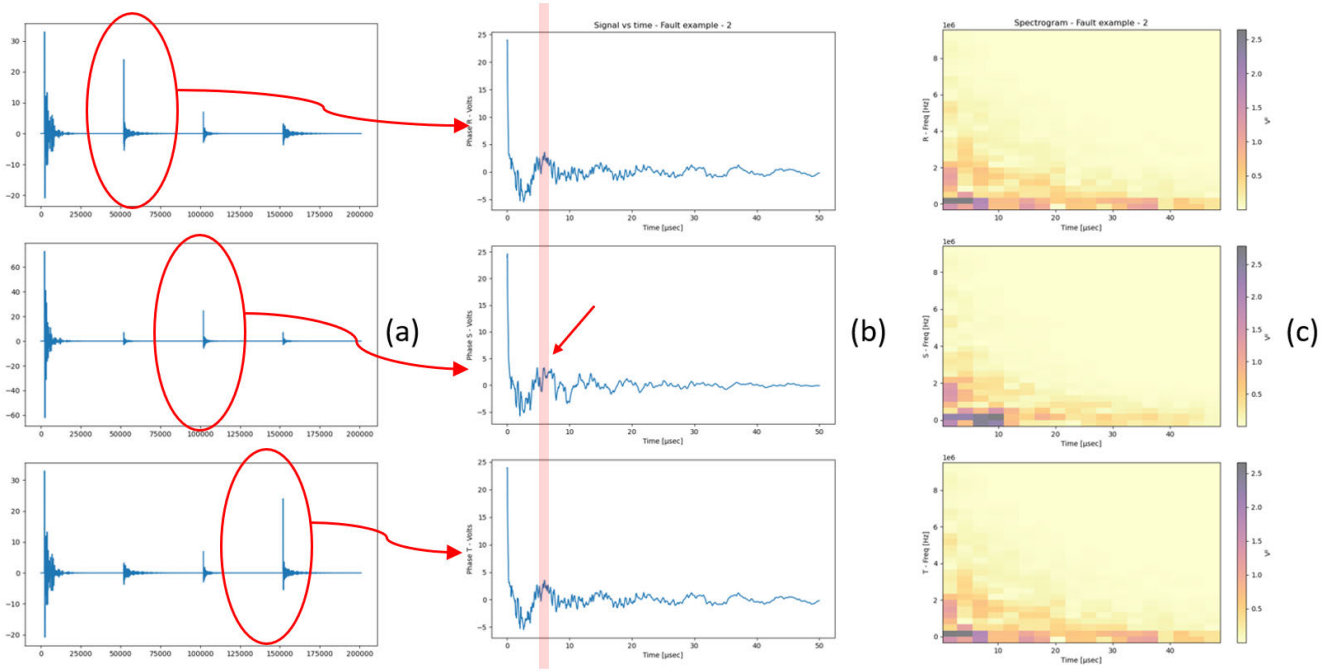

FIGURE 40. Fault signal Type 2 (Top-Phase R / Middle-Phase S / Bottom-Phase T). (a) Complete Injection, (b) Phase Injection, (c) Spectrogram.

In figures (39, 40, 41, 41, 42 and 43), it can be seen how the first signal that appears is the fault event itself. This means that the simulator simulates the short-circuit of the phase(s) to ground and a ''spike'' is produced as a consequence of the short-circuit. Then, a necessary time is waited for the event to extinguish. This is necessary to avoid injecting when traces of the fault spike signal are still present in the network. This would cause our injected pulse to have noise and give us erroneous information about the state of the network. Obviously, in Figure 38, there is no such signal from the fault event since that is the case where we inject a pulse into the network without a fault.

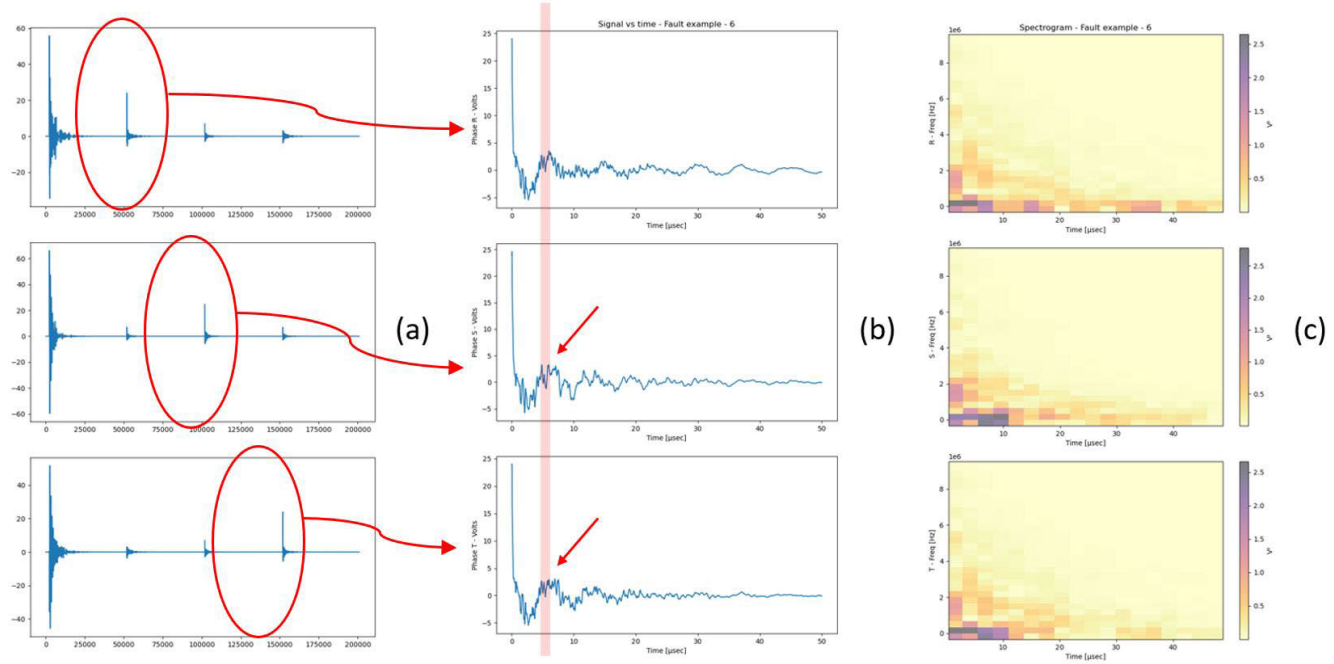

FIGURE 41. Fault signal Type 3 (Top-Phase R / Middle-Phase S / Bottom-Phase T). (a) Complete Injection, (b) Phase Injection, (c) Spectrogram.

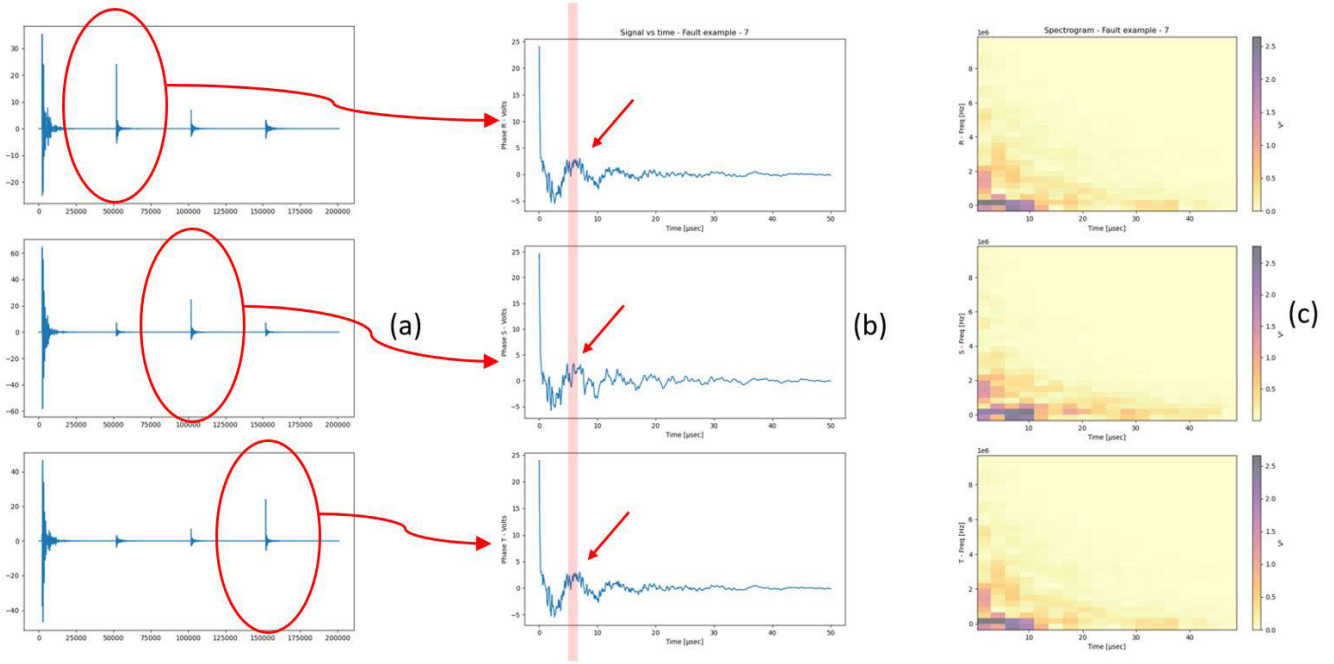

FIGURE 42. Fault signal Type 4 (Top-Phase R / Middle-Phase S / Bottom-Phase T). (a) Complete Injection, (b) Phase Injection, (c) Spectrogram.

In each one of the phases, the injected pulse is marked with a red circle. The injection process is as follows. A first pulse is injected in the S phase (red circle in the upper signal). This pulse is also induced in the other two phases (S and T). After waiting a certain time for the injected pulse to die out, another pulse is injected, but this time in the S phase (red circle in the middle signal). Which is also induced in the other two phases (R-T). Finally, another pulse is injected in the T phase (red circle in the bottom signal).

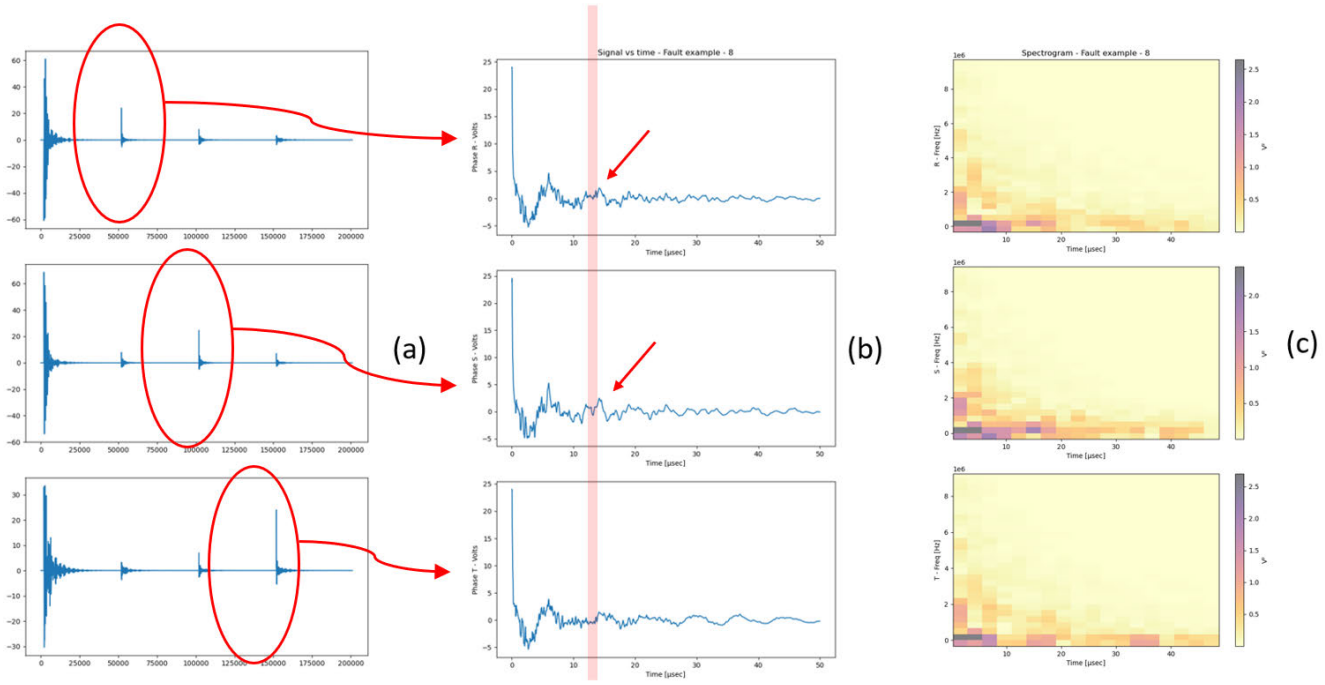

FIGURE 43. Fault signal Type 5 (Top-Phase R / Middle-Phase S / Bottom-Phase T). (a) Complete Injection, (b) Phase Injection, (c) Spectrogram.

This injection sequence is intended to avoid mixing the injected signals with those induced from the other phases, which would lead to erroneous signals.

In this process, each time a pulse is injected, the response of the signal bounced by the network is sampled (at the same injection point). In this way, at the end of the three injections, we will have 3 buffers with the response signal of each of the phases, thus discarding the rest of the induced signals that contain redundant information, as well the ''spike'' signal of the fault event.

In subfigure (b) we can see the three signals obtained from the previous process. In each of the figures, we have marked with a red stripe the time at which the rebound of the fault occurs and with a red arrow, the phase(s) in which the fault has occurred.

The first figure (Fig. 38) shows the response to the injected pulse of the modelled real network in its normal state (without any fault produced).

In the examples shown below, we have chosen the FT4 fault, which is located at about 933m and whose rebound should arrive at 6 μs after injection. The pulse travels about 300m/us, but it has to go to the fault and bounce back to the injection point, so it has to travel the distance to the fault twice so, the fault bounce should show some peculiar characteristic at about 6 μs.

Each of the other figures (Fig. 39, 40, 41, and 42), the response of each type of fault is shown. Thus, we should find in the vicinity of those 6 μs differences between the responses of each type of fault and that of the pre-fault. Moreover, these differences should be consistent with the type of fault, i.e., the differences should appear in those phases in which the fault occurred and not in the rest.

In Fig. 41, we have chosen the fault FT6, which is at about 1833m, to have another example at a different distance. In this case, the rebound should arrive at about 12 μs, so we should see some difference with the pre-fault signal around that time.

As can be seen in the figures, around the distance to the fault, a ''subtle'' difference between the pre-fault and fault signals can be appreciated. Moreover, as we expected, this difference occurs only in those phases in which the foul has occurred, while in the rest, the fault and pre-fault signals are practically identical.

It can be seen how the differences between the signals have a very small amplitude, which is mixed with the rest of the ''peaks'' that appear over time, and which correspond to each impedance change that the injected signal encounters on its way. Thus, as already explained, the fault is one more impedance variation in the line.

In the spectrogram, we can see how around the zone where the fault occurs (6 us), we have signals of several frequencies with the highest amplitudes to decay with time. This agrees with the time signal and with the theory since, at the beginning, the bounced signal still has enough energy. This energy disappears over time due to the attenuation of the signal as it travels along the line.

We can also observe in the spectrogram, as there is a relatively low frequency (KHz) that is present and that is due to the resonance of the coupler to the pulse injection. This signal plays the role of ''carrier'' on which is ''mounted'' the information of the ''bounces'' of the injected pulse. As it

does not contain information on the network status, this low frequency signal can be eliminated in the post-processing.

As a conclusion, as we have already mentioned, we can say that these variations are not at all obvious and reflect the complexity of extracting the classification of the type of fault, as well as its precise location. For the location accuracy to be less than 15 m, we would have to make a location error of less than 0.1 μs (the time it takes for a pulse to travel the distance of 30 m (15 m out and 15 m back). As can be seen, an error of 0.1 μs in 6 μs equals approximately 1.6%.

With this study of the signals, we can conclude that the information of interest is embedded in the response of the network to the pulse injection. With these simulated signals from a real network, we can, therefore, develop algorithms that allow us to classify and/or locate the faults. Later in the future, we can verify them when the real faults occur in the selected network where the pulse injector has been installed.

VII. CONCLUSION

As mentioned above, there are data from different power grids of varying complexity and age, most of them supported by the IEEE Power & Energy Society. Even though all of them provide a very good test bed for experiments with power failures, we believe that new techniques and scenarios require more complex data and there have been great advances in this line of research because of this initiative.

Therefore, we are confident that the new proposal based on the TDR principle can offer new insights, and additionally, creating and providing ready-made data for processing by researchers not directly linked to the electrical field can provide a strong boost to advances in this sector.

On the other hand, the shared data have been obtained with a simulation software, PSCAD^{TM}, with great potential and capacity to perform highly complex studies. We think it is a very good alternative at the moment when no real power failure signals are available, because fortunately no such incidents have occurred in an in-service network. But high-quality signals are available thanks to this software, very similar to those expected when such incidents occur in the future.

Finally, since this is purely experimental research, a couple of applications have been carried out in which the know-how obtained has been put into practice. On the one hand, a prototype has been installed (as shown in Fig. 29, Fig. 30 and Fig. 31) inside an existing installation, and on the other hand, the simulated data obtained have been processed for the classification of electrical faults [47] using the latest techniques of pattern recognition and deep learning.

In summary, the main points of our study are as follows:

- Simulate a real electrical network in PSCAD to obtain a database of 200 simulated fault signals.
- Install a prototype pulse injector (TDR) in that modeled real installation to be able to record real signals.
- And a real system ready to collect real data of electrical incidents. In this way, it is possible to populate and compare the results obtained in the immediate future from simulated signals with responses to future real signals.

VIII. FUTURE WORK

In the short-term work, the expectations from this work are:

- Possibility to compare in the future the signals obtained by simulation and synthesis with the signals recorded in the field.
- Verify if the detection and classification performed with these synthesized signals is able to train the system to be able to detect and classify the real signals recorded in the field.
- Populate with more examples that are consistent and of the same complexity as the original ones. In this way, and in the previous referenced work, a system for synthesized data generation is proposed, which is a suitable complement to the original data. All of these data is intended to be included in the same shared repository.

Talking about our future medium-term work, it will be focused on the TDR technique and on trying to explore and improve the limits that this phenomenon can provide us when identifying, and subsequently locating, faults with a higher impedance.

Together with the objective mentioned above, we want to focus on the problem of the presence of distributed generations in different distribution networks. Also, in applications where detection/localization is required in greater distance ranges, playing with different injection frequencies, or even considering multipoint injection systems.

On the other hand, and with our own experience gained from our previous works, the objective of obtaining a target fault location system, and with the highest possible accuracy, becomes indispensable. This objective could not be achieved without the progress we are currently making in the definition and formalization of simulation systems. These systems provide us with the seed with which to produce training data that will provide us with the minimum capacity to meet the localization challenge.

REFERENCES

[1] L. Peretto, R. Tinarelli, A. Bauer, and S. Pugliese, "Fault location in underground power networks: A case study," in *Proc. ISGT*, 2011, pp. 1–6, Accessed: Mar. 30, 2022. [Online]. Available: https://ieeexplore-ieee-org.cuarzo.unizar.es:9443/document/5759198/

[2] A. Bahmanyar, S. Jamali, A. Estebsari, and E. Bompard, "A comparison framework for distribution system outage and fault location methods," *Electric Power Syst. Res.*, vol. 145, pp. 19–34, Apr. 2017.

[3] J.-H. Teng, W.-H. Huang, and S.-W. Luan, "Automatic and fast faulted line-section location method for distribution systems based on fault indicators," *IEEE Trans. Power Syst.*, vol. 29, no. 4, pp. 1653–1662, Jul. 2014, doi: 10.1109/TPWRS.2013.2294338.

[4] M. A. López, "Algoritmos de localización de faltas en redes eléctricas," Doctoral dissertation, 2016.

[5] S. Robson, A. Haddad, and H. Griffiths, "Fault location on branched networks using a multiended approach," *IEEE Trans. Power Del.*, vol. 29, no. 4, pp. 1955–1963, Aug. 2014, doi: 10.1109/TPWRD.2014.2302137.

[6] K. Sun, Q. Chen, and Z. Gao, "An automatic faulted line section location method for electric power distribution systems based on multisource information," *IEEE Trans. Power Del.*, vol. 31, no. 4, pp. 1542–1551, Aug. 2016, doi: 10.1109/TPWRD.2015.2473681.

[7] S. Lotfifard, M. Kezunovic, and M. J. Mousavi, "A systematic approach for ranking distribution systems fault location algorithms and eliminating false estimates," *IEEE Trans. Power Del.*, vol. 28, no. 1, pp. 285–293, Jan. 2013, doi: 10.1109/TPWRD.2012.2213616.

[8] R. J. Hamidi and H. Livani, "Traveling-wave-based fault-location algorithm for hybrid multiterminal circuits," *IEEE Trans. Power Del.*, vol. 32, no. 1, pp. 135–144, Feb. 2017, doi: 10.1109/TPWRD.2016.2589265.

[9] A. Farughian, L. Kumpulainen, and K. Kauhaniemi, "Review of methodologies for earth fault indication and location in compensated and unearthed MV distribution networks," *Electric Power Syst. Res.*, vol. 154, pp. 373–380, Jan. 2018, doi: 10.1016/j.epsr.2017.09.006.

[10] P. Stefanidou-Voziki, N. Sapountzoglou, B. Raison, and J. L. Dominguez-Garcia, "A review of fault location and classification methods in distribution grids," *Electric Power Syst. Res.*, vol. 209, Aug. 2022, Art. no. 108031, doi: 10.1016/j.epsr.2022.108031.

[11] K. Yang, R. Zhang, J. Yang, Y. Chen, and S. Chen, "Research on low-voltage series arc fault detection method based on least squares support vector machine," *Open Electr. Electron. Eng. J.*, vol. 9, no. 1, pp. 408–421, Sep. 2015, doi: 10.2174/1874129001509010408.

[12] D. Bisht and A. Bhandakkar, "Shunt faults detection on transmission line: A review," *Int. J. Elect. Electron. Res.*, vol. 3, no. 4, 2015, Accessed: Feb. 16, 2023. [Online]. Available: https://www.researchpublish.com/papers/shunt-faults-detection-on-transmission-line-a-review

[13] S. S. Gururajapathy, H. Mokhlis, and H. A. Illias, "Fault location and detection techniques in power distribution systems with distributed generation: A review," *Renew. Sustain. Energy Rev.*, vol. 74, pp. 949–958, Jul. 2017, doi: 10.1016/j.rser.2017.03.021.

[14] Y. Q. Chen, O. Fink, and G. Sansavini, "Combined fault location and classification for power transmission lines fault diagnosis with integrated feature extraction," *IEEE Trans. Ind. Electron.*, vol. 65, no. 1, pp. 561–569, Jan. 2018, doi: 10.1109/TIE.2017.2721922.

[15] J. Oasa, M. Yamanaka, S. Higashiyama, Y. Inaoka, T. Hisakado, O. Wada, T. Matsushima, T. Hirayama, and K. Yamaoka, "Verification of fault location by TDR measurement on an actual line including multiple ground-mounted equipment," in *Proc. 26th Int. Conf. Exhib. Electr. Distrib.*, 2021, pp. 1274–1278.

[16] R. Lacoste, *Robert Lacoste's The Darker Side: Practical Applications for Electronic Design Concepts From Circuit Cellar*. 2010, pp. 33–47, doi: 10.1016/B978-1-85617-762-7.00003-4.

[17] Y. Miyoshi and S. Saba, "Some features and performances of type C transmission-line fault locators," *Trans. Amer. Inst. Electr. Eng. III, Power App. Syst.*, vol. 76, no. 3, pp. 445–451, Apr. 1957, doi: 10.1109/AIEEPAS.1957.4499585.

[18] E. Herrero, J. Granado, and A. Llombart, "CVLAB-UNIZAR/CIRCE_fault_database: Initial release," Tech. Rep., Nov. 2022, doi: 10.5281/ZENODO.7316010.

[19] F. J. L. Padua and R. De Oliveira, "Allocation of PLC devices in a low-voltage grid," in *Proc. IEEE PES Innov. Smart Grid Technol. Conf.-Latin Amer.*, Sep. 2019, pp. 1–4, doi: 10.1109/ISGT-LA.2019.8895457.

[20] R. Dashti, S. Salehizadeh, H. Shaker, and M. Tahavori, "Fault location in double circuit medium power distribution networks using an impedance-based method," *Appl. Sci.*, vol. 8, no. 7, p. 1034, Jun. 2018, doi: 10.3390/app8071034.

[21] M. Shafiullah and M. A. Abido, "S-transform based FFNN approach for distribution grids fault detection and classification," *IEEE Access*, vol. 6, pp. 8080–8088, 2018, doi: 10.1109/ACCESS.2018.2809045.

[22] A. Aljohani, A. Aljurbua, M. Shafiullah, and M. A. Abido, "Smart fault detection and classification for distribution grid hybridizing ST and MLP-NN," in *Proc. 15th Int. Multi-Conference Syst., Signals Devices (SSD)*, Mar. 2018, pp. 94–98, doi: 10.1109/SSD.2018.8570582.

[23] A. Ekka and A. Yadav, "Fault identification using fuzzy in renewable energy interfaced IEEE 13 bus system," in *Proc. Int. Conf. Intell. Controller Comput. Smart Power*, 2022, pp. 1–6, doi: 10.1109/ICICCSP53532.2022.9862498.

[24] G. R. Kumar. *Estimation and Minimization of Harmonics in IEEE 13 Bus Distribution System*. Accessed: Nov. 23, 2022. [Online]. Available: www.ijert.org

[25] B. Ahmed, A. Abdelgadir, N. A. Saied, and A. A. Karrar, "A compensated distributed-parameter line decoupling approach for real time applications," *IEEE Trans. Smart Grid*, vol. 12, no. 2, pp. 1761–1771, Mar. 2021, doi: 10.1109/TSG.2020.3033145.

[26] K. P. Schneider, B. A. Mather, B. C. Pal, C. W. Ten, G. J. Shirek, H. Zhu, J. C. Fuller, J. L. R. Pereira, L. F. Ochoa, L. R. de Araujo, and R. C. Dugan, "Analytic considerations and design basis for the IEEE distribution test feeders," *IEEE Trans. Power Syst.*, vol. 33, no. 3, pp. 3181–3188, Oct. 2017, doi: 10.1109/TPWRS.2017.2760011.

[27] W. H. Kersting, "Radial distribution test feeders distribution system analysis subcommittee report," in *Proc. IEEE Power Eng. Soc. Winter Meeting*, Feb. 2001, pp. 908–912, Accessed: Nov. 23, 2022. [Online]. Available: http://ewh.ieee.org/soc/pes/dsacom/testfeeders.html

[28] M. Scarpetta, M. Spadavecchia, G. Andria, M. A. Ragolia, and N. Giaquinto, "Analysis of TDR signals with convolutional neural networks," in *Proc. IEEE Int. Instrum. Meas. Technol. Conf. (IMTC)*, May 2021, pp. 1–6, doi: 10.1109/I2MTC50364.2021.9460009.

[29] D. Nagata, S. Fujioka, T. Matshushima, H. Kawano, and Y. Fukumoto, "Detection of fault location in branching power distribution network using deep learning algorithm," in *Proc. Int. Symp. Electromagn. Compat.*, Sep. 2022, pp. 655–660, doi: 10.1109/EMCEUROPE51680.2022.9901205.

[30] D. Haddad, A. Y. Kallel, N. E. B. Amara, and O. Kanoun, "Multiple faults detection and location in bus-shaped cable networks by distributed time-domain reflectometry," *IEEE Sensors Lett.*, vol. 6, no. 5, pp. 1–4, May 2022, doi: 10.1109/LSENS.2022.3170645.

[31] S. Thomas, "Antenna system measurements using frequency domain reflectometry vs. time domain reflectometry," in *Proc. IEEE Autotestcon*, Sep. 2006, pp. 230–236, doi: 10.1109/AUTEST.2006.283643.

[32] A. Tengg and P. Hank, "Reflectrometry based fault localization in automotive bus systems," in *Proc. IEEE Int. Instrum. Meas. Technol. Conf.*, Mar. 2012, pp. 397–402, doi: 10.1109/I2MTC.2012.6229648.

[33] X. Gu, "On-line test and fault location of aviation general-purpose cables based on TDR," in *Proc. 3rd Int. Conf. Comput. Vis., Image Deep Learn. Int. Conf. Comput. Eng. Appl.*, May 2022, pp. 294–297, doi: 10.1109/CVIDLICCEA56201.2022.9825377.

[34] M. Ziwei and W. Xueye, "A portable railway signal cable fault detector," in *Proc. 5th Int. Conf. Inf. Sci., Comput. Technol. Transp. (ISCTT)*, Nov. 2020, pp. 69–72, doi: 10.1109/ISCTT51595.2020.00021.

[35] M. Hampe, M. Tetzlaff, and T. Müller, "Analytical method to check and correct the TDR impedance profile of low-loss transmission lines," in *Proc. Int. Symp. Electromagn. Comput.*, Sep. 2022, pp. 740–743, doi: 10.1109/EMCEUROPE51680.2022.9901087.

[36] J. Mora-Flòrez, J. Meléndez, and G. Carrillo-Caicedo, "Comparison of impedance based fault location methods for power distribution systems," *Electr. Power Syst. Res.*, vol. 78, no. 4, pp. 657–666, Apr. 2008, doi: 10.1016/j.epsr.2007.05.010.

[37] C. Galvez and A. Abur, "Fault location in active distribution networks containing distributed energy resources (DERs)," *IEEE Trans. Power Del.*, vol. 36, no. 5, pp. 3128–3139, Oct. 2021, doi: 10.1109/TPWRD.2020.3034179.

[38] H. Mirshekali, R. Dashti, A. Keshavarz, A. J. Torabi, and H. R. Shaker, "A novel fault location methodology for smart distribution networks," *IEEE Trans. Smart Grid*, vol. 12, no. 2, pp. 1277–1288, Mar. 2021, doi: 10.1109/TSG.2020.3031400.

[39] X. Lin, F. Zhao, G. Wu, Z. Li, and H. Weng, "Universal wavefront positioning correction method on traveling-wave-based fault-location algorithms," *IEEE Trans. Power Del.*, vol. 27, no. 3, pp. 1601–1610, Jul. 2012, doi: 10.1109/TPWRD.2012.2190108.

[40] C.-C. Zhou, Q. Shu, and X.-Y. Han, "A single-phase earth fault location scheme for distribution feeder on the basis of the difference of zero mode traveling waves," *Int. Trans. Electr. Energy Syst.*, vol. 27, no. 5, p. e2298, May 2017, doi: 10.1002/ETEP.2298.

[41] W. Chonglin, W. Yangyang, L. Rui, and S. Gang, "Fault location for single-phase-to-earth faults based on transient traveling wave method and artificial pulse signal injection method," in *Proc. Int. Conf. Electr. Control Eng.*, Jun. 2010, pp. 3737–3741. [Online]. Available: https://ieeexplore-ieee-org.cuarzo.unizar.es:9443/document/5629889/

[42] M. Abad, S. Borroy, D. Lopez, and M. Garciagracia, "New fault location method for up-to-date and upcoming distribution networks," in *Proc. CIRED*, 2015, pp. 15–18.

[43] J. Livie, P. Gale, and A. Wang, "Experience with on-line low voltage cable fault location techniques in Scottish power," in *Proc. 19th Int. Conf. Electr. Distrib.*, 2007, pp. 1–4.

[44] M. A. Aftab, S. M. S. Hussain, I. Ali, and T. S. Ustun, "Dynamic protection of power systems with high penetration of renewables: A review of the traveling wave based fault location techniques," *Int. J. Electr. Power Energy Syst.*, vol. 114, Jan. 2020, Art. no. 105410, doi: 10.1016/j.ijepes.2019.105410.

[45] R. Benato and A. Paolucci, "Operating capability of long AC EHV transmission cables," *Electric Power Syst. Res.*, vol. 75, no. 1, pp. 17–27, Jul. 2005, doi: 10.1016/J.EPSR.2004.11.011.

[46] C. A. Nucci, F. Rachidi, and M. Rubinstein, "Derivation of telegrapher's equations and field-to-transmission line interaction," *WIT Trans. State Art Sci. Eng.*, vol. 29, pp. 1755–8336, Jan. 2008, doi: 10.2495/978-1-84564-063-7/01.

[47] J. G. Fornas, E. H. Jaraba, A. L. Estopinan, and J. Saldana, "Detection and classification of fault types in distribution lines by applying contrastive learning to GAN encoded time-series of pulse reflectometry signals," *IEEE Access*, vol. 10, pp. 110521–110536, 2022, doi: 10.1109/ACCESS.2022.3214994.

JAVIER GRANADO FORNÁS received the B.Sc. degree in industrial engineering (specialized in industrial electronics) and the M.Sc. degree in electronics engineering (intelligent environments specialization) from the University of Zaragoza, Spain, in 1994 and 2014, respectively. He is currently pursuing the Ph.D. degree in deep learning around the classification and localization of faults in distribution lines. Since 2009, he has been a Senior Researcher with the Electronics Systems Group, CIRCE Technology Center. His main research interests include electronic design control projects around deep learning and algorithms for fault detection.

ELÍAS HERRERO JARABA (Member, IEEE) received the Ph.D. degree in engineering from the University of Zaragoza, in June 2005.

He has been a Professor with the University of Zaragoza, since 2002. In 1999, he worked in the automotive field with the Production Department, Opel Spain, for four years. Within the university, he has developed his research in the area of computer vision, and since 2012, he has been focused his interest on the field of neural networks, and more recently, in deep learning. In the meantime, he held the position of coordinator of the Smart Vehicle Initiative with the Aragon Institute for Engineering Research (I3A). He currently holds a European patent and has led to more than six projects funded in public competitions, more than 20 projects with companies, 12 indexed publications, and more than 50 contributions to international conferences. He is currently developing his research career within the research group "Human OpenWare Research Lab (Howlab)." His teaching work has focused on electronics, from its basics to power electronics, including embedded systems.

Dr. Jaraba received the 3M Award for his research in the CvLAB Research Group.

HANS BLUDSZUWEIT was born in Jena, Germany, in 1974. He received the Dipl.-Ing. degree in electrical engineering from the Technical University of Ilmenau, Germany, in 2001, and the Ph.D. degree (European Doctorate) in electrical engineering from the University of Zaragoza, Spain, in 2009. He worked as a Field Test Engineer on the sector of solar PV module production with First Solar, for one year. Since 2009, he has been a Researcher in the field of electrical systems with CIRCE, where he is currently a Technological Expert with the Smart Grid Operation Group. His activity is focused on smart grids (optimization of distributed resources, including storage and statistical analysis of Smart Meter data) and grid integration of electric vehicles, including dynamic wireless charging (e-roads).

DAVID CERVERO GARCÍA received the B.Sc. degree in industrial engineering (specializing in electric systems) and the M.Sc. degree in renewable energies and energy efficiency from the University of Zaragoza, in 2009 and 2011, respectively.

Currently, he is a Project Manager with the Electronic Systems Group, CIRCE Technology Centre. He has a deep expertise in power quality (PQ) assessment in electrical systems, data acquisition, especially in digital signal processing, developing dedicated software for measuring PQ in electrical distribution networks and the performance of renewable energy sources. His research interests include fault location and power systems monitoring, with an application in predictive maintenance. Currently, his main research field is focused on designing resonant converters for high-voltage applications.

ANDRÉS LLOMBART ESTOPIÑAN (Member, IEEE) received the industrial engineering degree from the University of Zaragoza, in 1994, and the Ph.D. degree in electrical engineering from the University of Zaragoza, in 2000.

He has been the General Director of CIRCE, since April 2016, and the former Executive Director, since January 2011. He was also a Lecturer with the Electrical Department, University of Zaragoza, from June 2003 to May 2018. In November 2011, he was designated by the Science and Innovation Ministry as the Expert of the Energy Area Committee of the7th Funding Program of the European Union, being in charge of the coordination of electricity grid topics. In CIRCE, he is in charge of the Innovation and Promotion Unit, created by himself, in May 2009. From March 2007 to March 2009, he was the Subdirector of the Institutional Relations of the Superior Polytechnic Centre, University of Zaragoza. Later, he researched the impact reduction of power electronic source grids using passive filters in the kilowatt range. From December 1994 to May 2001, he was an Associate Professor with the Electrical Engineering Department, University of Zaragoza, where he performed the following teaching activities: electric circuit theory, industrial actuation, wind energy, and renewable energy integration. He participated in more than 35 R&D+i projects; in 16 of them, he was the primary researcher. He has authored ten articles in indexed journals and more than 50 contributions to international congresses. His active participation in forums, associations, and platforms is linked to activity lines. He holds eight patents, of which seven are being exploited.